Hyperon electroproduction in a crossing and duality constrained model

Robert A. Williams, Chueng-Ryong Ji, and Stephen R. Cotanch
North Carolina State University, Raleigh, North Carolina 27695
(Received 20 April 1992)

Using our previously developed crossing and duality consistent model for kaon photoproduction and radiative capture, we investigate the kaon electroproduction processes $p(e,e'K^+)Y$ for $Y=\Lambda$, Σ^0, and $\Lambda(1405)$. Because there is no electroproduction data near threshold, consistency requires extending the energy range of our photoproduction model parametrization from an upper bound of $E_\gamma^{\rm lab}=1.4$ to 2.2 GeV. We find that baryon resonances with spin greater than $\frac{1}{2}$ are necessary to describe the higher energy photoproduction data ($1.4\leq E_\gamma^{\rm lab}\leq 2.2$ GeV). We also extend our use of duality by representing these higher-spin s- and u-channel baryon resonances with the low-lying t-channel vector, $K^*(890)$, and pseudovector, $K_1(1270)$, mesons. Using this extended crossing and duality consistent model, we obtain reasonable agreement with the data for both photoproduction and electroproduction processes.

PACS number(s): 13.60.−r, 11.50.Jg, 12.40.Lk

I. INTRODUCTION

Electroproduction processes are widely recognized as important for investigating the electromagnetic structure and excitation of the nucleon. Although clearly related to photoproduction, electroproduction reactions have several distinctions which make them particularly useful and interesting. The most notable feature is that electron scattering is mediated by "massive" virtual photons ($q^2\neq 0$). By specifying the electron beam energy and final-state electron angle, the experimentalist can fix the virtual photon's invariant mass (q^2) and degree of transverse or longitudinal polarization. Probing hadronic systems with virtual photons provides additional insight into the basic reaction mechanism (resonance formation, polarization and interference effects, etc.) and also to fundamental hadronic structure information (electromagnetic form factors).

In this paper we extend our crossing and duality constrained hadron pole model for kaon photoproduction, $p(\gamma,K^+)Y$ for $Y=\Lambda$, Σ^0, and $\Lambda(1405)$ [1], to higher energies while generalizing it for the corresponding electroproduction processes, $p(e,e'K^+)Y$. In Sec. II, we review the dynamical content of our model which implements crossing and duality constraints. The electroproduction formalism is summarized in Sec. III. Here we emphasize covariance which directly facilitates analytic continuation necessary for incorporating crossing. In Sec. IV we compare our numerical results with available electroproduction data and discuss the significance and consistency of our fitted parameters. Finally, we conclude in Sec. V with a discussion of our model limitations and future directions for hyperon electromagnetic production phenomenology.

II. MODEL DETAILS

We employ a relativistic hadron pole model, which is based on an effective field chiral Lagrangian evaluated at the tree level, and establish a consistent phenomenology by utilizing crossing and duality constraints. Crossing and duality impose restrictions which limit the number and type of diagrams allowed. The model parameters are the electromagnetic and strong coupling constants, which, in general, have not yet been uniquely determined. In a recent analysis [2], we reported a crossing and duality constrained set of parameters that were determined by simultaneously fitting kaon photoproduction and radiative capture data in both the Λ and Σ^0 reaction channels. In this analysis, we will test these parameters by generalizing our calculations to compare with the existing electroproduction data, which fortunately includes the production of not only Λ and Σ^0, but also the $\Lambda(1405)$ (in constrast with photoproduction). These reaction channels are interrelated and complimentary, with each process involving diagrams with different combinations of the same coupling constants, therefore a comprehensive analysis should provide a more reliable set of parameters. Before discussing our numerical results we detail the distinguishing features of our model.

A. Duality and crossing

Duality is a hypothesized property of hadronic interactions that has well-established phenomenological support and far-reaching theoretical implications. Dolen, Horn, and Schmid [3] found that interference models, which include resonances in both s (u) and t channels simultaneously, entail double counting and are therefore an overcomplete description for the low-energy π-N scattering. Moreover, they were able to infer several features of the high-energy amplitudes utilizing analyticity via the finite-energy sum rule (FESR). Specifically, they were able to extract the t-channel ρ Regge trajectories, which govern the asymptotic high-energy behavior, based purely on the s-channel N^* resonances of their low-energy model. This curious result lead to the concept of a "duality" between s- (u-) and t-channel resonances in π-

N scattering, and eventually to the speculation that all hadronic interactions may share this property. Mathematicians formalized the duality principle and developed so-called "dual models," such as the crossing symmetric Veneziano amplitude [4], that exhibit duality exactly. The analytic description of duality is intimately related with Regge pole theory. Poles in the t channel, which in Regge theory determines the asymptotic high-energy behavior, arise from divergences in the fixed-t dispersion integral in the s channel (i.e., the FESR). These divergences appear in the amplitude because an infinite number of resonances are implicitly summed along each Regge trajectory. In this way, duality relates families of resonances on Regge trajectories in the s (u) and t channels. For a comprehensive review of duality, we refer the reader to Refs. [5] and [6].

Although the extent to which duality is satisfied is not experimentally clear for all hadronic reactions, duality does have a long history of phenomenological applications, with several notable successes. With regard to hyperon electromagnetic processes, the most extensive duality based study was made by Renard and Renard [7], who applied the FESR to $K^+\Lambda$ and $K^+\Sigma^0$ photoproduction processes. They found that their low-energy amplitude, which included only s- and u-channel graphs (with several resonances up to J=7/2), successfully reproduced average features of the high-energy amplitude based on Reggeized K^* and K^{**} t-channel exchanges. Encouraged by their results, we have incorporated duality into our model describing hyperon production. In our previous low-energy study [1] we performed a passive application of duality by simply requiring that all resonances in the t channel should be excluded as they are "dual" to s- and u-channel resonances. This type of duality constraint has also been implemented in other investigations [2, 8], but is too restrictive for higher-energy studies, which require, in general, resonances with spin greater than 1/2. Without such resonances, the model will develop a deficiency in partial waves at higher energies. We present a more detailed discussion of this point in Sec. IV. Because of the necessity to include many higher-spin resonances to simulate t-channel poles, only nonminimal models such as in Ref. [7] that include every possible resonance up to arbitrarily large spin can consistently apply a passive duality constraint over a wide range of energies.

In order to preserve simplicity and phenomenological efficiency (i.e., to describe the largest set of data with the fewest possible parameters) we now choose to apply duality more aggressively by including the low-lying t-channel K^* resonances which, when combined with the poles of our model s- and u-channel graphs, generate an improved intermediate energy behavior. In particular, we include the lowest-mass t-channel resonances [the $J^\pi = 1^-$ $K^*(890)$ and the $J^\pi = 1^+$ $K_1(1270)$] along with the kinematically enhanced, spin-1/2 s- and u-channel resonances. Our use of duality is fundamentally motivated to optimize truncation and minimize double counting. Because only a few low spin resonances on different Regge trajectories are included in our new minimal model, double counting is not a problem. Further, the passive use of duality (i.e., to neglect all t-channel graphs) leads to deficiencies in models limited to the lowest-spin resonances, because the higher-spin resonances, which are important for simulating the t-channel poles, are never incorporated. In this way, our original photoproduction model was somewhat oversimplified and only appropriate near threshold (where t-channel poles have little effect). However, in our new extended model we no longer passively apply duality by attempting to sum on the higher-spin resonances of specified Regge trajectories, rather, we add only kinematically enhanced spin-1/2 states (i.e., across trajectories with poles inside the energy range of our database), and include the vector and pseudovector kaons which simulate the higher-spin baryon resonances which have been omitted. We still view this use of duality as a constraint which simplifies the model by reducing the number of necessary diagrams required for a consistent phenomenology. More fundamentally, duality provides a theoretical framework for identifying the equivalence of K^* t-channel resonances with a collective average of the neglected s- and u-channel (N^*, Δ^*, and Y^*) states. We acknowledge that other researchers also have demonstrated the importance of these spin-1 kaons in electromagnetic hyperon production (within the same pole model formalism) [9].

The other dynamic constraint which we incorporate, crossing, is well appreciated and requires little justification. Crossing is an exact symmetry of the S matrix that relates reactions involving particles (antiparticles) in the initial/final state with reactions where the corresponding antiparticles (particles) are in the final/initial state [10]. For this study the crossing related reactions are kaon photoproduction, (γ, K^+), and radiative capture (K^-, γ). Because these reactions are governed by the same dynamical mechanism (i.e., involve the same set of covariant diagrams), any realistic parametrization must apply simultaneously for both of these processes. Conversely, if a model parametrization is incapable of describing both crossing related channels then it is deficient (i.e., unphysical). All of the parametrizations which we employ yield calculated kaon capture branching ratios within the reported errors of the recent data [11] and are therefore consistent with the crossing constraint. For additional details on crossing and on its application as a constraint in phenomenological studies, the reader is refered to Refs. [1], [2], and [10].

B. Resonances in a "minimal model"

In our model for low-energy kaon electromagnetic production the photon (real or virtual) couples directly to the proton, kaon, final-state strange baryon, and certain excited resonances of these hadrons. A meaningful phenomenological description for this type of mechanism must identify and incorporate the proper set of resonances which mediate the production. This is why the use of duality in a minimal model can be such a powerful principle. Instead of trying to assess the relative importance of individual resonances, duality allows one t-channel pole to represent a collective average of an entire set of higher-spin direct channel resonances. This

produces a much smaller parameter space, and therefore the phenomenologically extracted coupling constants become very tightly constrained and much more reliable.

Alternative approaches which attempt to include all possible resonances are plagued with complexity, ambiguity, and uncertainty. Although a complete understanding of the basic reaction mechanism depends on assessing the relative importance of each participating resonance, it is impossible to unambiguously determine individual resonance contributions with the presently available data. Ideally, phenomenological studies should include all possible contributing resonances, fixing all the known parameters and then let the fitting algorithm determine the remaining parameters. However, in practice there are several problems with this approach. By design, this type of description is very complicated, requiring several parameters and an abundance of accurate experimental information for several observables over a wide kinematic range. Unfortunately, most of the current cross section data are concentrated at forward angles and distributed unevenly in energy (with most of the photoproduction data ranging from $0.9 \leq E_\gamma^{\rm lab} \leq 1.5$ GeV, and the electroproduction data ranging from about $2.0 \leq E_\gamma^{\rm lab} \leq 2.5$). The available polarization data are scarce and of questionable quality, which, at best, provides only a weak consistency check on the fitted parameters. Furthermore, even with the concentrated historical effort, none of the strong coupling constants, including the Born $KN\Lambda$ and $KN\Sigma$, are well established and therefore all parameters should be considered adjustable [confining the Born couplings to be consistent with $SU(3)_f$ or hadronic scattering determinations is suspect due to the uncertainties of both unbroken $SU(3)_f$ and severe approximations in purely hadronic models]. As evidenced by the large number of existing parametrizations, several equivalent sets of coupling constants have been found for (γ, K^+) with substantially different numerical values. Most of these competing sets can be ruled out by their lack of consistency with cross-channel data, however we stress the necessity for new data in both kaon capture and production channels, with a special emphasis on polarization observables which are particularly sensitive to individual resonance contributions. Nevertheless, progress is still possible by comprehensively using all of the available information in every related reaction channel while utilizing reliable dynamic constraints in a model which captures the essential physics.

In Fig. 1, we summarize the resonances which define our minimal model. The criteria for diagram selection is the following: (a) spin-1/2 baryons with masses that generate kinematic enhancement for the energies analyzed; and (b) low-lying strange mesons having spin 1 which are treated as dual to baryon resonances with angular momentum greater than 1/2. We assume that spin-1/2 intermediate states in the direct channel, either below threshold or with a mass greater than $\sqrt{s_{\rm max}}$, are negligible. We consider the photoproduction data below $\sqrt{s_{\rm max}}$ = 2.3 GeV (cutoff laboratory photon energy at 2.25 GeV), which is comparable in energy with the electroproduction data. For Λ production, $N^*(1650)$ and $N^*(1710)$

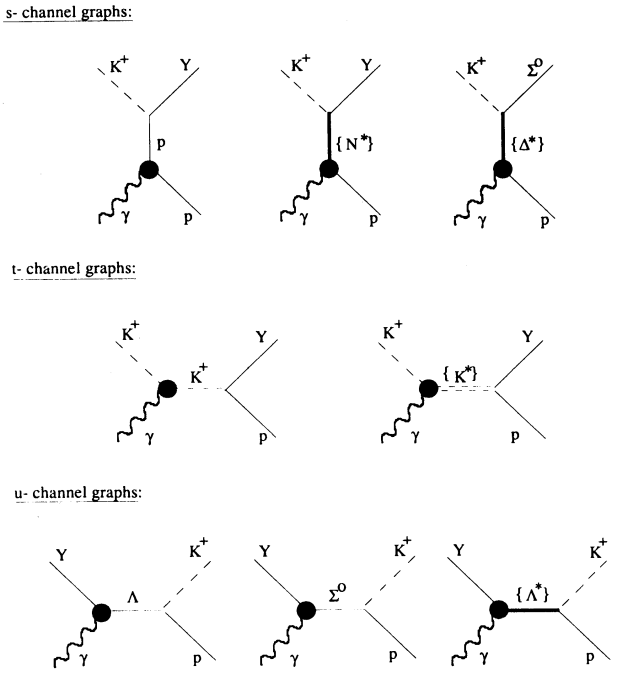

FIG. 1. Diagrams used in our model for (γ, K^+) and (K^-, γ). $\{N^*\} \equiv \{N(1650), N(1710)\}$, $\{\Lambda^*\} \equiv \{\Lambda(1405)\}$, $\{\Delta^*\} \equiv \{\Delta(1620), \Delta(1900), \Delta(1910)\}$, $\{K^*\} \equiv \{K^*(892), K_1(1270)\}$.

are the only resonant s-channel states that qualify (see Fig. 1). For Σ production, isospin conservation permits the additional $\Delta^*(1620)$, $\Delta^*(1900)$, and $\Delta^*(1910)$ states to enter. In the u channel, we include only the $\Lambda(1405)$ resonance because under crossing the low-energy capture process is dominated by this state [12].

III. ELECTROPRODUCTION FORMALISM

The formalism for electroproduction is well developed in other papers [13, 14]; we include a discussion of the essential details. Here we present a covariant expression for the transition amplitude and provide relations for the kinematic invariants in a frame convenient for our calculations. To establish notation, we write

$$e(e_1) + p(p) \longrightarrow e'(e_2) + K^+(k) + Y(l) \qquad (1)$$

where the four-momentum for each particle is written inside the parentheses and the virtual photon momentum is defined to be $q = e_1 - e_2$. Within the one-photon-exchange approximation, the transition amplitude can be expressed as the invariant product of leptonic, $J_{\mathcal{L}}$, and hadronic, $J_{\mathcal{H}}$, currents mediated by the photon propagator:

$$t_{fi} = \frac{J_{\mathcal{L}} \cdot J_{\mathcal{H}}}{q^2} \ . \qquad (2)$$

These currents are the matrix elements of appropriate operators:

$$J^{\mu}_{\mathcal{L}} = < e^{'} \mid \hat{J}^{\mu}_{\mathcal{L}} \mid e > = e\ \bar{u}_{e'}(e_2, s_2)\ \gamma^{\mu}\ u_e(e_1, s_1) \equiv \mathcal{L}^{\mu}\ , \tag{3}$$

and

$$J^{\mathcal{H}}_{\mu} = < K^{+}\ Y \mid \hat{J}^{\mathcal{H}}_{\mu} \mid p > = \bar{u}_{Y}(l, \lambda^{'})\ [\sum_{i=1}^{6} A_i \mathcal{M}^{i}_{\mu}\ ]\ u_p(p, \lambda) \equiv \mathcal{H}_{\mu}\ . \tag{4}$$

The hadronic current operator is expanded in terms of the Lorentz invariant elementary amplitudes, $A_i(q^2, s, t, u)$, which are scalar functions of the Mandelstam variables $s = (q+p)^2$, $t = (q-k)^2$, and $u = (q-l)^2$, multiplying the explicitly gauge-invariant bilinear matrices $(\mathcal{M}^{i}_{\mu})$. The choice of a particular set of bilinear covariants is not unique and therefore the hadronic current operator can be expanded in terms of a different basis such as

$$\sum_{i=1}^{6} A_i \mathcal{M}^{i}_{\mu} = \sum_{j=1}^{6} B_j \mathcal{N}^{j}_{\mu}\ , \tag{5}$$

with one particular choice for $\mathcal{M}$ and $\mathcal{N}$ written explicitly as

$$\begin{aligned}
\mathcal{M}^1_\mu(\pm) &= \frac{1}{2}\Gamma_{(\pm)}(\not{l}\,\gamma_\mu - \gamma_\mu \not{l}), & \mathcal{N}^1_\mu(\pm) &= \frac{1}{2}\Gamma_{(\pm)}(\not{q}\,\gamma_\mu - \gamma_\mu \not{q}),\\
\mathcal{M}^2_\mu(\pm) &= 2\Gamma_{(\pm)}(l\cdot q\, p_\mu - p\cdot q\, l_\mu), & \mathcal{N}^2_\mu(\pm) &= \Gamma_{(\pm)}(p_\mu - \frac{p\cdot q}{q^2}\, q_\mu),\\
\mathcal{M}^3_\mu(\pm) &= \Gamma_{(\pm)}(p\cdot q\,\gamma_\mu - \not{q}\, p_\mu), & \mathcal{N}^3_\mu(\pm) &= \Gamma_{(\pm)}(l_\mu - \frac{l\cdot q}{q^2}\, q_\mu),\\
\mathcal{M}^4_\mu(\pm) &= \Gamma_{(\pm)}(l\cdot q\,\gamma_\mu - \not{q}\, l_\mu), & \mathcal{N}^4_\mu(\pm) &= \Gamma_{(\pm)}(p\cdot q\,\gamma_\mu - \not{q}\, p_\mu),\\
\mathcal{M}^5_\mu(\pm) &= 2\Gamma_{(\pm)}(p-l)^\nu(q_\mu q_\nu - q^2 g_{\mu\nu}), & \mathcal{N}^5_\mu(\pm) &= \Gamma_{(\pm)}(l\cdot q\,\gamma_\mu - \not{q}\, l_\mu),\\
\mathcal{M}^6_\mu(\pm) &= \Gamma_{(\pm)}(\not{q}\, q_\mu - q^2\,\gamma_\mu), & \mathcal{N}^6_\mu(\pm) &= \Gamma_{(\pm)}(\not{q}\, q_\mu - q^2\,\gamma_\mu),
\end{aligned} \tag{6}$$

where the matrix $\Gamma_{(\pm)}$ depends on whether the produced hyperon has even or odd parity:

$$\Gamma_{(\pm)} = \begin{cases} \gamma_5 \text{ if } \pi_Y = + \ \{Y = \Lambda, \Sigma^0\}, \\ \mathbf{1} \text{ if } \pi_Y = - \ \{Y = \Lambda(1405)\}. \end{cases} \tag{7}$$

The $\mathcal{M}^j$ basis is a generalization of the 4 photoproduction covariants, with $\mathcal{M}^5$ and $\mathcal{M}^6$ containing the new spin degrees of freedom for the virtual photon. This basis permits a transparent comparison of the virtual versus real photoproduction cross section formula. The $\mathcal{N}^j$ basis is useful for simplifying the Feynman diagram calculations of the invariant amplitudes (B_j), and therefore we adopt it for this purpose. The 6×6 basis transformation matrix is given in the Appendix, where we also write the generalized invariant amplitude expressions.

The differential electroproduction cross section involves the spin averaged, squared transition amplitude multiplying the three-body phase-space kinematic factors:

$$d\sigma = \frac{(2\pi)^{-5} M_p\ M_Y\ M_e^2}{2\ [(e_1\cdot p)^2 - M_e^2 M_p^2]^{\frac{1}{2}}} < |t_{fi}|^2 > \delta(e_1 + p - e_2 - k - l) \frac{d\mathbf{e}_2 d\mathbf{k}\ d\mathbf{l}}{E_{e'}\ E_k\ E_Y}\ . \tag{8}$$

Integrating over the hyperon three-momentum gives

$$\sigma^3 \equiv \frac{d^3\sigma}{d\Omega_{e'}\ dE_{e'}\ d\Omega_k} = \frac{(2\pi)^{-5} M_p\ M_Y\ M_e^2\ |\mathbf{k}|^2\ E_{e'}}{2\ [(e_1\cdot p)^2 - M_e^2 M_p^2]^{\frac{1}{2}} E_k\ E_Y\ R} < |t_{fi}|^2 > \tag{9}$$

where

$$R = \frac{\mathbf{k}}{|\mathbf{k}|}\cdot\left(\frac{\mathbf{k}}{E_k} - \frac{\mathbf{l}}{E_Y}\right).$$

The spin averaged, squared transition matrix is a covariant quantity, given by the following expressions:

$$< |t_{fi}|^2 > = \frac{1}{4} \sum_{s_1,s_2} \sum_{\lambda,\lambda'} |e\bar{u}_{e'}(e_2,s_2)\, \frac{\gamma_\mu}{q^2}\, u_e(e_1,s_1)\, \mathcal{H}^\mu|^2 \tag{10}$$

$$= \frac{e^2}{4q^4 M_e^2} \sum_{\lambda,\lambda'} [\, 2\, |\mathcal{H}\cdot e_1|^2 \,+\, \frac{1}{2} q^2 |\mathcal{H}|^2\,] \tag{11}$$

derived using the spin algebra trace theorems, current conservation (which eliminates the e_2 dependence), and various kinematic relations. Defining the usual electromagnetic fine structure constant $\alpha_e \equiv \frac{e^2}{4\pi} = \frac{1}{137}$, and substituting the explicit hadronic current [Eqs. (4) and (7)] yields the following:

$$< |t_{fi}|^2 > = (\frac{\pi \alpha_e}{8 M_Y\, M_p\, M_e^2})\, (\frac{1}{q^2}) \sum_{i,j=1}^{6} A_i A_j^*\, [\, T_1^{ij} + T_2^{ij}] \tag{12}$$

with

$$T_1^{ij} \equiv \mathrm{Tr}\, [\, (\not{l} + M_Y)\mathcal{M}_\mu^i (\not{p} + M_p)\mathcal{M}_\nu^{j\dagger}\, g^{\mu\nu}\,] \tag{13}$$

and

$$T_2^{ij} \equiv (\frac{4}{q^2})\, \mathrm{Tr}\, [\, (\not{l}+M_Y)(\mathcal{M}^i\cdot e_1)(\not{p}+M_p)(\mathcal{M}^{j\dagger}\cdot e_1)]\ . \tag{14}$$

All traces have been performed using REDUCE, giving the T_1^{ij} and T_2^{ij} matrix elements listed in the Appendix.

A particularly useful form of Eq. (9) is derived when the lepton kinematics are evaluated in the laboratory frame, current conservation is applied to eliminate one of the current components (scalar or longitudinal), and the square amplitude evaluated. Choosing the following coordinate system (see Fig. 2)

$$\begin{aligned} \hat{\mathbf{z}} &= \frac{\mathbf{q}}{|\mathbf{q}|}\ , \\ \hat{\mathbf{y}} &= \mathbf{e}_1 \times \frac{\mathbf{e}_2}{|\mathbf{e}_1 \times \mathbf{e}_2|}\ , \\ \hat{\mathbf{x}} &= \hat{\mathbf{y}} \times \hat{\mathbf{z}} \end{aligned} \tag{15}$$

and defining

$$\begin{aligned} \epsilon &\equiv \frac{1}{(1 - \frac{2\mathbf{q}^2}{q^2} \tan^2 \frac{\Psi}{2})}, \\ \epsilon_L &\equiv -\frac{q^2}{q_0^2}\epsilon \end{aligned} \tag{16}$$

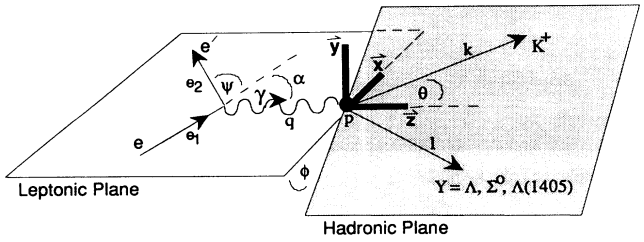

FIG. 2. Laboratory frame kinematics for electroproduction.

which measures the virtual photon's degree of transverse and longitudinal polarization respectively as a function of the laboratory electron scattering angle Ψ, the averaged square amplitude can be re-expressed as

$$< |t_{fi}|^2 > = (\frac{e^2}{4q^4 M_e^2})\, (\frac{2q^2}{\epsilon - 1}) \sum_{i,j=1}^{3} \rho^{ij} \Theta_{ij}\ . \tag{17}$$

The Θ and ρ matrices are defined by

$$\Theta_{ij} \equiv \frac{1}{2} \sum_{\lambda,\lambda'} \mathcal{H}_i^* \mathcal{H}_j \tag{18}$$

which is the matrix formed by the independent (spin averaged) hadronic current components, and

$$(\rho^{ij}) \equiv \begin{pmatrix} \frac{1}{2}(1+\epsilon) & 0 & -[\frac{1}{2}\epsilon_L(1+\epsilon)]^{1/2} \\ 0 & \frac{1}{2}(1-\epsilon) & 0 \\ -[\frac{1}{2}\epsilon_L(1+\epsilon)]^{1/2} & 0 & \epsilon_L \end{pmatrix} \tag{19}$$

which is the virtual photon polarization density matrix. Finally, because all of the leptonic dependence in the phase space can be factorized, the electroproduction differential cross section can be related to the (virtual) photoproduction cross section $\frac{d\sigma_v}{d\Omega_k}$:

$$\sigma^3 = \Phi\, \frac{d\sigma_v}{d\Omega_k} \tag{20}$$

where

$$\Phi = \frac{\alpha_e E_{e'} [(q\cdot p)^2 - q^2 M_p^2]^{1/2}}{2\pi^2 [(e_1\cdot p)^2 - M_e^2 M_p^2]^{1/2} q^2 (\epsilon - 1)} \tag{21}$$

and

$$\frac{d\sigma_v}{d\Omega_k} = \frac{\mathbf{k}^2\, M_p\, M_Y}{16\pi^2 [(q\cdot p)^2 - q^2 M_p^2]^{1/2} E_k\, E_Y\, R} \times \sum_{i,j=1}^{3} \rho^{ij} \Theta_{ij}. \tag{22}$$

Φ is interpreted to be the virtual photon flux seen in the proton's rest frame. In the center-of-momentum frame, the cross-section formula simplifies further:

$$\frac{d\sigma_v^{\text{c.m.}}}{d\Omega_k} = \frac{|\mathbf{k}|}{|\mathbf{q}|}\frac{M_p\, M_Y}{16\pi^2\, s} < |\mathcal{T}_{fi}|^2 > \tag{23}$$

where $< |\mathcal{T}_{fi}|^2 >$ is defined to be the virtual photoproduction square averaged amplitude:

$$< |\mathcal{T}_{fi}|^2 > \equiv \sum_{i,j=1}^{3} \rho^{ij}\Theta_{ij}. \tag{24}$$

Notice that this squared virtual photoproduction amplitude, which is a Lorentz-invariant quantity for real photoproduction, is not covariant for electroproduction due to the frame dependence of the polarization parameter ϵ (i.e., the degree of transverse or longitudinal polarization is not invariant under a Lorentz boost). Obviously, the polarization density matrix and the hadronic current matrix are evaluated in the specific laboratory frame defined by Eq. (15). We have found a generalized form of Eq. (24) which clearly demonstrates how the covariance of the square amplitude for virtual photoproduction is broken and then restored in the limit as $q^2 \to 0$. The square amplitude takes the form

$$< |\mathcal{T}_{fi}|^2 > \equiv (\epsilon - 1) \sum_{\mu,\nu=1}^{4} \Lambda^{\mu\nu}\Theta_{\mu\nu} \tag{25}$$

where the $\Lambda^{\mu\nu}$ and $\Theta_{\mu\nu}$ are the covariant tensors formed by the leptonic and hadronic currents, respectively:

$$\begin{aligned}\Lambda^{\mu\nu} &\equiv \left(\frac{2M_e^2}{e^2q^2}\right) \sum_{s_1,s_2} \mathcal{L}^{\mu^*}\mathcal{L}^{\nu} \\ &= g^{\mu\nu} + \frac{2}{q^2}(e_1^{\mu}e_2^{\nu} + e_2^{\mu}e_1^{\nu}),\end{aligned} \tag{26}$$

$$\begin{aligned}\Theta_{\mu\nu} &\equiv \frac{1}{2}\sum_{\lambda,\lambda'} H_{\mu}^{*}H_{\nu} \\ &= \frac{A_iA_j^*}{8M_YM_p}\text{Tr}\,[\,(\not{p} + M_p)\mathcal{M}_{\mu}^{i\dagger}(\not{l} + M_Y)\mathcal{M}_{\nu}^{j}\,].\end{aligned} \tag{27}$$

The frame dependence of Eq. (25) is contained in the polarization parameter (ϵ) as an overall factor. A more general expression for ϵ relates the degree of transverse polarization to the x-y asymmetry in Λ:

$$\epsilon \equiv \frac{\Lambda^{11} - \Lambda^{22}}{\Lambda^{11} + \Lambda^{22}} \tag{28}$$

Of course this expression yields Eq. (16) when evaluated in the laboratory system.

The leptonic tensor can be re-expressed in the following form:

$$\Lambda^{\mu\nu} = g^{\mu\nu} + \left(\frac{\Sigma^{\mu}\Sigma^{\nu} - q^{\mu}q^{\nu}}{q^2}\right) , \tag{29}$$

where Σ^{μ} is defined by

$$\Sigma^{\mu} \equiv (e_1^{\mu} + e_2^{\mu}) . \tag{30}$$

Before a direct comparison can be made between the virtual and real photoproduction amplitudes, the hadronic current tensor must first be averaged over all orientations of the leptonic and hadronic scattering planes (i.e., virtual photoproduction has an extra degree of freedom associated with ϕ):

$$\tilde{\Theta}_{\mu\nu} \equiv \frac{1}{\pi}\int_0^{\pi} \Theta_{\mu\nu}\, d\phi . \tag{31}$$

This integration is equivalent to projecting the off-diagonal (ϕ dependent) elements of Θ to zero. By applying current conservation and using the general definition of ϵ, the following limit can be established:

$$\lim_{q^2\to 0} \left[\, \Sigma^{\mu}\Sigma^{\nu} + q^2\left(\frac{\epsilon}{\epsilon - 1}\right)g^{\mu\nu} \,\right] \tilde{\Theta}_{\mu\nu} = 0 , \tag{32}$$

from which it follows that

$$\begin{aligned}\lim_{q^2\to 0}\ \Lambda^{\mu\nu}\,\tilde{\Theta}_{\mu\nu} &= \lim_{q^2\to 0}\left[\, g^{\mu\nu} + \left(\frac{\Sigma^{\mu}\Sigma^{\nu} - q^{\mu}q^{\nu}}{q^2}\right)\,\right]\tilde{\Theta}_{\mu\nu} \\ &= \left[g^{\mu\nu} - \left(\frac{\epsilon}{\epsilon - 1}\right)g^{\mu\nu}\,\right]\tilde{\Theta}_{\mu\nu} \\ &= \left(\frac{1}{1-\epsilon}\right) g^{\mu\nu}\Theta_{\mu\nu} ,\end{aligned} \tag{33}$$

where we have used current conservation ($q^{\mu}\Theta_{\mu\nu} = 0$) and the fact that $|\mathcal{H}|^2$ is independent of ϕ ($g^{\mu\nu}\tilde{\Theta}_{\mu\nu} = g^{\mu\nu}\Theta_{\mu\nu}$). Finally, the virtual photoproduction square amplitude becomes

$$\frac{1}{\pi}\int_0^{\pi} d\phi < |\mathcal{T}_{fi}|^2 > \overset{q^2\to 0}{\longrightarrow} -\frac{1}{2}\sum_{\lambda\lambda'} g^{\mu\nu}\,\mathcal{H}_{\mu}^{*}H_{\nu} , \tag{34}$$

which is precisely the covariant, real photoproduction result.

A useful identity for the virtual photoproduction cross section involves a decomposition into factors where the ϕ dependence is explicit:

$$\frac{d\sigma_v}{d\Omega_k} = \frac{d\sigma_U}{d\Omega_k} + \epsilon\frac{d\sigma_P}{d\Omega_k}\sin^2\theta\cos 2\phi + \epsilon_L\frac{d\sigma_L}{d\Omega_k} + [2\epsilon_L(\epsilon + 1)]^{1/2}\frac{d\sigma_I}{d\Omega_k}\sin\theta\cos\phi . \tag{35}$$

The U, P, L, and I terms are called the unpolarized transverse, polarized transverse, longitudinal, and interference cross sections, respectively. By expanding the squared amplitude using Eq. (24), the meaning of this terminology becomes clear:

$$< |\mathcal{T}_{fi}|^2 > = \sum_{\lambda,\lambda'} \left[\, \frac{1}{2}(|H_x|^2 + |H_y|^2) + \frac{\epsilon}{2}(|H_x|^2 - |H_y|^2) + \epsilon_L|H_z|^2 - [2\epsilon_L(\epsilon + 1)]^{1/2}(H_z^*H_x + H_x^*H_z)\,\right]. \tag{36}$$

The respective correspondence with the terms from the previous equation is obvious. Most of the experimental data involves only the U and L terms (i.e., averaged over all ϕ angles), hence this formula is useful for an efficient numerical evaluation of the σ_{UL} cross section, but it requires a direct calculation of the hadronic current components in the laboratory frame. Otherwise, if the covariant expressions are utilized [i.e., Eq. (12)], the various polarization dependent U, P, L, and I components can be projected out of the total squared amplitude by integrating over ϕ [using the orthogonality of $\cos(n\phi)$].

A. Electromagnetic form factors

Besides requiring additional spin degrees of freedom in the production amplitude, virtual photons probe the electromagnetic structure of the participating hadrons (via form factors). In a phenomenological model, such as this one, care must be taken to incorporate form factors which accurately represent the available data. This ensures that when model predictions are compared with the electroproduction data, deficiencies can be attributed to the dynamics and/or uncertainties in the unconstrained form factors. Within the framework of a purely hadronic model, the vector meson dominance (VMD) hypothesis provides the most natural and consistent description of the electromagnetic form factors. In VMD, the virtual photon can directly couple to any vector meson having the same quantum numbers and 4-momentum (e.g., ρ, ϕ, ω, etc.). When the photon interacts with a hadron, the strong vector meson interactions are assumed to "dominate" the direct coupling of the photon to the hadron. This assumption is known to be satisfied very well in the timelike q^2 region where very dramatic resonance features are observed in the pion and kaon form factors when the photon mass is near the mass of a vector meson. However, the VMD picture must at some point break down in the spacelike region where, at high q^2, the form factors will be dominated by the photon's direct coupling to the quarks [i.e., governed by perturbative QCD (PQCD)]. Therefore, we adopt the extended vector meson dominance (EVMD) model proposed by Gari and Krumpelmann, which is able to retain the successful VMD physics in the timelike region and also permit a smooth transition to the spacelike, high-q^2 scaling behavior of PQCD [15]. We stress that the formulas derived from EVMD manifestly respect crossing symmetry and are therefore applicable for both spacelike and timelike photon momentum transfers. This is difficult to achieve in other models and is important for our complimentary (K^-, e^+e^-) reaction studies which we will report in a future publication. It should be noted that even within the EVMD formalism there are several possible variations (including the use of "exact" propagators, radiative corrections, and multiple vector mesons) which may be investigated [16–18]. For now, we employ the simplest, phenomenologically acceptable EVMD form factors.

For the proton electric and magnetic form factors, $G_E^p(q^2)$ and $G_M^p(q^2)$, respectively, we use the EVMD parametrization of Gari and Krumpelmann [15]. Following their derivation, the most general EVMD expression for the kaon $[F_{K^+}(q^2)]$ charge form factor is found to be

$$F_{K^+}(q^2) = \gamma F_\gamma(q^2) + \sum_v F_v(q^2)\left(\frac{g_v}{f_v}\right)\frac{M_v^2}{M_v^2 - q^2 - iM_v\Gamma_v}, \quad (37)$$

where M_v and Γ_v are the mass and width of the vector meson, respectively, γ is a normalization constant, g_v/f_v is the effective vector meson coupling of the second graph in Fig. 3, and $F_v(q^2)$ is the intrinsic form factor associated with the hadronic vertex. $F_\gamma(q^2)$ is the form factor associated with the direct coupling of the photon to the hadron (first term in Fig. 3), and is therefore responsible for the transition to high-q^2 PQCD behavior. Both F_v and F_γ are normalized to 1 at $q^2 = 0$. The same formula applies to the K^*K transition form factor (with possibly different parameters), but it must be multiplied by the K^*K transition moment (due to its different normalization). At $q^2 = 0$, the kaon charge form factor is normalized to unity, which determines the constant γ:

$$\gamma + \sum_v \frac{g_v}{f_v} = 1. \quad (38)$$

Notice that the simple VMD model is equivalent to EVMD with a sum rule on the coupling constants (i.e., $\gamma = 0$) and all strong form factors taken to be constant. Obviously, Eq. (37) has much more flexibility than simple VMD, with the inclusion of strong coupling form factors and an additional term allowing for direct photon contributions. This additional freedom is precisely what is needed to accurately represent the nucleon electric and magnetic form factors (which follow a dipole scaling law) using a VMD prescription. For spin-0 mesons (such as K^+), the experimental form factor data are well described by monopole scaling, which is consistent with simple VMD [i.e., $\gamma = 0$, and $F_v(q^2) = 1$]. The three parameters for the kaon form factor are well determined by the known $\phi \to K^+K^-$ decay width plus two normalization constraints [$F_{K^+}(q^2 = 0) = 1$, and $F_{K^0}(q^2 = 0) = 0$], yielding charge radii for the K^+ and K^0 within experimental uncertainties ($< r^2_{K^+} >= 0.335$ fm^2 and $< r^2_{K^0} >= -0.058$ fm^2). The resulting parameters are given in the first column of Table I. To our knowledge, there is no experimental information on the K^*K transition form factor, therefore for simplicity we assume no dependence on the strong form factor [i.e., $F_v(q^2) = 1$] as with the kaon, but allow for direct coupling with the

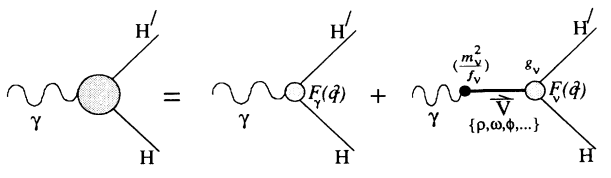

FIG. 3. Extended vector meson dominance (EVMD) picture of a physical photon coupling to a hadron.

TABLE I. EVMD coupling constants for the K^* transition and K^+ charge form factors.

EVMD coupling	$K^+K^+\gamma$	$K^*K\gamma$
g_ρ/f_ρ	0.5	0.5
g_ω/f_ω	0.17	0.17
g_ϕ/f_ϕ	0.33	0.77
g_{ϕ^*}/f_{ϕ^*}	0.0	0.63

photon (i.e., $\gamma \neq 0$). We acknowledge the ambiguity in the K^*K^+ transition form factor; however, we emphasize that all other coupling constants and form factors are well justified. Assuming our model has the correct dynamical content for electroproduction at intermediate energies, we can extract the K^*K^+ transition form factor, taking advantage of sensitivity to the K^* graphs, by fitting the available data with all other parameters fixed. In addition to the ρ, ω, and ϕ vector mesons, we include the excited $\phi^*(1680)$ meson which has a large decay width in the $K^*(890)K^+$ channel. We assume universality of the nonstrange (ρ and ω) vector meson couplings [19] and hence there are two independent parameters, g_ϕ/f_ϕ and g_{ϕ^*}/f_{ϕ^*}, which we adjust to give the best fit to the electroproduction data. In our calculations, we use the same monopole form factor associated with the photon used by Gari and Krumpelmann [i.e., $F_\gamma(q^2) = \frac{\lambda^2}{\lambda^2 - q^2}$ with $\lambda \sim 0.8$ GeV]. The resulting parameter set, representing our prediction for the K^*K^+ transition form factor, is listed in the second column of Table I. For simplicity we have assumed the same q^2 behavior for both the $K^*(890)K^+\gamma$ and $K_1(1270)K^+\gamma$ transitions.

Electromagnetic form factors can be introduced into our photoproduction amplitudes by the following replacements at each electromagnetic vertex. For the γpp vertex

$$e \longrightarrow e_p = e\, G_E^p(q^2),$$

with the anamolous magnetic moment

$$\mu_p \longrightarrow \mu_N\, [G_M^p(q^2) - 1].$$

For the γK^+K^+ vertex

$$e \longrightarrow e_K = e\, F_{K^+}(q^2).$$

For the γK^*K^+ vertex

$$g_{K^*K\gamma} \longrightarrow g_{K^*K\gamma} F_{K^*K}(q^2).$$

For the $\gamma BB'$ vertex

$$\mu_{BB'} \longrightarrow \mu_{BB'} \left(\frac{G_M^p(q^2)}{G_M^p(0)}\right).$$

It should be noted that we have implicitly used the same $G_M(q^2)$ for all baryons, which may be regarded as an additional approximation.

In principle, form factors should also be included at the strong interaction vertices to account for the composite nature of the hadrons manifest at large momentum transfer. In this study, as a first approximation, we neglect this effect and consider only energy independent hadronic couplings. This should be a good approximation for the KN^*Y interactions since for the energies considered in this analysis the N^* resonances propagate nearly on shell and thus transfer little momentum. However, this assumption may not be well satisfied for the nonresonant Born diagrams since these graphs are far off shell even near threshold. The historical neglect of this effect in electromagnetic production studies may, in part, account for the long-standing discrepancy of the extracted Born $KN\Lambda$ and $KN\Sigma$ coupling constants when compared with either $SU(3)_f$ predictions (which relate on-shell couplings) or determinations from low-energy KN elastic scattering (which either extract these couplings much closer to their on-shell values or else explicitly include monopole form factors, producing a suppression of the meson exchange with increasing momentum transfer [20, 21]). In this study, we do not include this effect, choosing rather to avoid the ambiguity and uncertainties associated with introducing additional parameters into the model. However, because this off-shell suppression is probably not negligible at the energies considered here, we regard our extracted g_{KNY} coupling constants to be representative values evaluated at some average 4-momentum transfer. Of course this is not a precise definition because this "average" momentum transfer is different for the diagrams in each channel, $< s > -M_p^2 \sim 3$ GeV^2, $< t > -M_K^2 \sim -0.4$ GeV^2, and $< u > -M_\Lambda^2 \sim -2.6$ GeV^2, but at least we have a qualitative understanding for why the extracted couplings are consistently suppressed relative to the values obtained from KN scattering or $SU(3)_f$ predictions.

IV. NUMERICAL RESULTS AND DISCUSSION

In Table II, we compare the effective coupling constants which we have determined in this and our previous analysis, sets (a) and (b) respectively. All magnetic parameters are reported in Bohr magnetons (i.e., $\frac{e\hbar}{2M_pc}$). It is interesting that the s- and u-channel resonance couplings seem to be fairly stable with respect to the inclusion of K^* graphs. This stability helps verify that the low-energy photoproduction data is dominated by the influence of only a few spin-1/2 resonances (those included in our previous model). In other words, the K^* graphs decouple from the low-energy production mechanism (ignoring the tendency for the K^* graphs to produce a larger coupling for the proton graph) as expected from duality. We note that our new coupling constants are in excellent agreement with the values obtained by Renard and Renard, giving further support for our implementation of duality. Before our results for electroproduction are given, we first display curves which demonstrate the failure of our "naive" low-energy minimal model and the subsequent success of our new model which now includes the $K^*(890)$ and $K_1(1270)$ in describing the photoproduction data for energies up to 2.25 GeV. In Figs. 4 and 5, the dot-dash curve represents our original model whereas the solid curve represents our new parametrization. The failure of our original

TABLE II. Coupling constants for (γ, K^+) and $(e, e'K^+)$.

		$Y = \Lambda$		$Y = \Sigma^0$		$Y = \Lambda(1405)$	
Diagram	Effective coupling	(a)	(b)	(a)	(b)	(a)	(b)
p, K^+	g_{KNY}	8.427	4.127	-0.968	-0.329	2.598	2.651
Λ	$\mu_{Y\Lambda} g_{KN\Lambda}$	-5.166	-2.530	13.359	6.657	1.161	-0.709
Σ^0	$\mu_{Y\Sigma} g_{KN\Sigma}$	-1.561	-0.531	-0.784	-0.266	0.813	0.281
$\Lambda(1405)$	$\mu_{Y\Lambda(1405)} g_{KN\Lambda(1405)}$	0.358	-0.451	-2.181	-2.237	-1.143	-1.166
$N(1650)$	$\mu_{N(1650)_P} g_{KN(1650)Y}$	0.213	0.453	-0.437	-0.426	28.062	15.489
$N(1710)$	$\mu_{N(1710)_P} g_{KN(1710)Y}$	0.323	0.875	-2.329	-2.143	-2.037	-1.915
$\Delta(1620)$	$\mu_{\Delta(1620)_P} g_{K\Delta(1620)Y}$	-	-	0.161	0.161	-	-
$\Delta(1900)$	$\mu_{\Delta(1900)_P} g_{K\Delta(1900)Y}$	-	-	0.315	0.315	-	-
$\Delta(1910)$	$\mu_{\Delta(1910)_P} g_{K\Delta(1910)Y}$	-	-	2.757	2.158	-	-
$K^*(892)$	$g_{K^*(892)K} g^V_{K^*(892)NY}$	2.032	0	-1.375	0	-0.399	0
	$g_{K^*(892)K} g^T_{K^*(892)NY}$	-0.984	0	1.774	0	-0.218	0
$K_1(1270)$	$g_{K_1(1270)K} g^V_{K_1(1270)NY}$	-0.236	0	1.684	0	0.581	0
	$g_{K_1(1270)K} g^T_{K_1(1270)NY}$	-2.175	0	-0.862	0	2.164	0

model becomes evident at higher (intermediate) energies whereas, by design, our new model is quite satisfactory at these energies. The curves for $\Lambda(1405)$ are omitted here because there is no photoproduction data available for comparison. The extension to electroproduction is now straightforward. Utilizing the same parameter sets, and using the EVMD form factors described earlier, we calculate the q^2, $W = \sqrt{s}$, and t dependence of our model for comparison with the data.

Figures 6, 7, and 8 display the q^2 dependence for Λ, Σ^0, and $\Lambda(1405)$ production respectively. The Λ and Σ^0 dependence on q^2 is reproduced very well; however, the $\Lambda(1405)$ behavior is slightly off, with our model showing dipole-like scaling, whereas the data follows more of

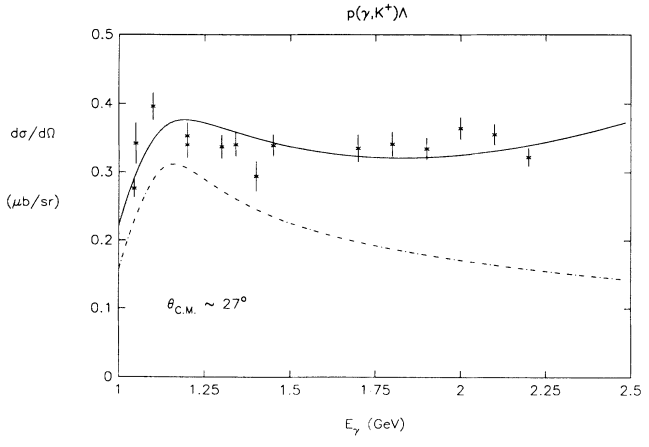

FIG. 4. $p(\gamma, K^+)\Lambda$ photoproduction cross section at $\theta_{\text{c.m.}} \sim 90°$. The solid curve represents our new model predictions while the dash-dotted curve represents our original model which excludes the $K^*(890)$ and $K_1(1270)$ graphs. Data are taken from Ref. [26] and references therein.

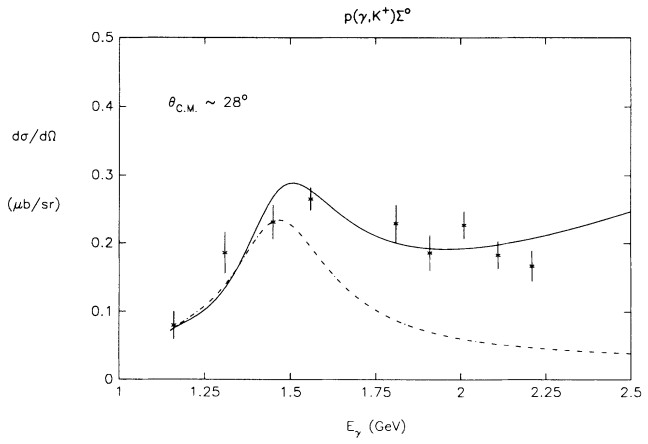

FIG. 5. $p(\gamma, K^+)\Sigma^0$ photoproduction cross section at $\theta_{\text{c.m.}} \sim 90°$ with curves labeled (and hereafter) as in Fig. 4. Data are taken from Ref. [26] and references therein.

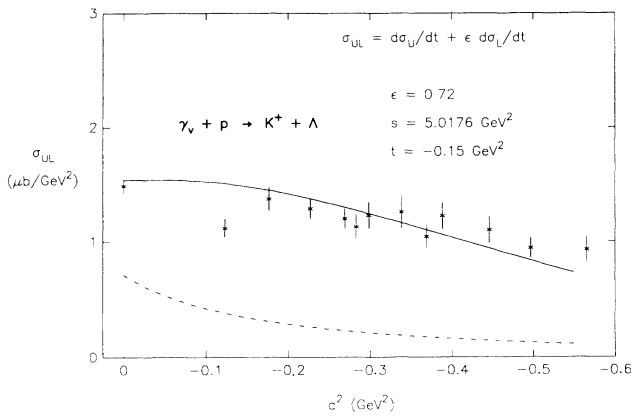

FIG. 6. Unpolarized virtual photoproduction cross section (σ_{UL}) for Λ as a function of q^2. Data are taken from Ref. [27] and references therein.

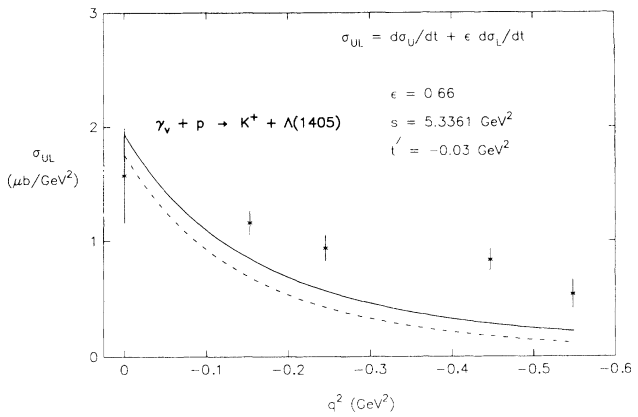

FIG. 8. Unpolarized virtual photoproduction cross section (σ_{UL}) for $\Lambda(1405)$ as a function of q^2. Data are taken from Ref. [27] and references therein.

a monopole q^2 dependence. We stress that, due to the large sensitivity to the K^* graphs for Λ and Σ^0 electroproduction, our model makes a definite, nontrivial prediction for the K^*K^+ transition form factor (with all other parameters previously fixed to the photoproduction data). Qualitatively, the transition form factor falls off more slowly than the K^+ charge form factor for spacelike momentum transfers. In the timelike region, the excited $\phi(1680)$ meson is a strong, broad resonance for the K^*K^+ transition whereas it decouples completely from the kaon form factor ($g_{\phi^* KK} = 0$).

It is worth noting that an improved q^2 description for the $\Lambda(1405)$ can easily be obtained by readjusting some of the unconstrained resonance parameters (only Born graph $\Lambda(1405)$ parameters are constrained by the Λ and Σ^0 photoproduction fits); however, this undermines the overall data set description by increasing the total χ^2. This demonstrates, however, that interference between diagrams can substantially modify the q^2 scaling behavior. We believe it is likely that interference from spin-1/2 u-channel Λ^* and Σ^* resonances which we have neglected may be important for $\Lambda(1405)$ production. This conclusion is supported by the extremely large value we obtain for the effective coupling of the $N^*(1650)$ graph, which implies our neglect of some important dynamic resonance(s).

Another interesting result is that while our original model (dot-dashed curve) underestimates the Λ and Σ^0 data by a factor of 2 or more (for all q^2), it is properly normalized for the $\Lambda(1405)$ data, especially at $q^2 = 0$ (see Figs. 8, 12, and 15), even if all resonance parameters are set equal to zero. The failure of our former low-energy model can be understood by examining Fig. 9 where the relative kaon-hyperon momentum is plotted as a function of the incident photon's laboratory energy. This figure indicates, for a given reaction, the necessary partial waves needed for a specific energy. The partial wave number L must satisfy the Bohr angular momentum quantization condition $\Delta|\mathbf{p}|\Delta|\mathbf{r}| \sim L\hbar$, where $\Delta|\mathbf{p}|$ is taken as the K-Y relative momentum and $\Delta|\mathbf{r}|$, the uncertainty in position, is the proton rms charge radius. From this estimation, a model including only s and p waves (as in our original model limited to spin-1/2 resonances) should be partial wave deficient at about 1.5 GeV for Λ and Σ^0 production where d-wave contributions become important. For $\Lambda(1405)$ production the deficiency energy is simply shifted upward 0.5 to about 2.0 GeV due to the difference between Λ and $\Lambda(1405)$ thresholds. This explains the apparently anomalous success of our original model in describing $\Lambda(1405)$ production near threshold while failing for Λ and Σ^0 production in the same energy region. The necessity of the K^* and K_1 mesons at higher energy is consistent with the need for additional partial waves at these energies for the Λ and Σ^0 but not for the $\Lambda(1405)$ since the limited $\Lambda(1405)$ electroproduction data exists only for photon energies between 2.0 and 2.5 GeV, where s and p waves are sufficient. Nevertheless, for consistency, we have also included these K^* graphs and have determined their vector and tensor couplings which further reduce the χ^2 (given by the solid curve in Figs. 8, 12, and 15). While this slightly improves the

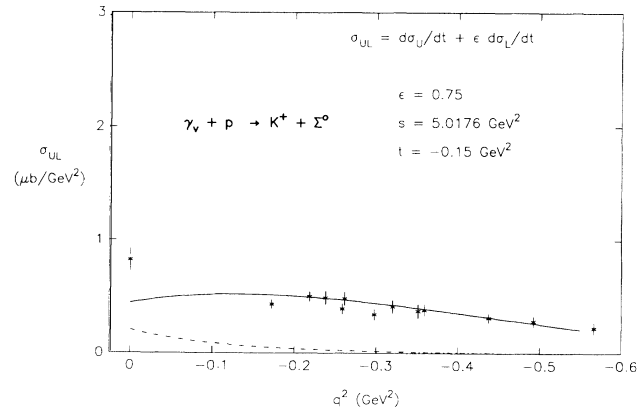

FIG. 7. Unpolarized virtual photoproduction cross section (σ_{UL}) for Σ^0as a function of q^2. Data are taken from Ref. [27] and references therein.

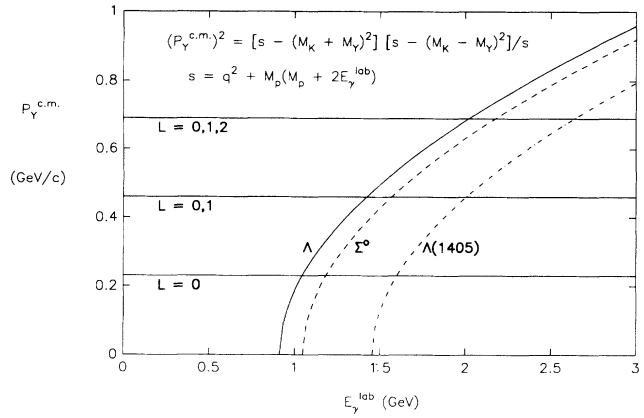

FIG. 9. K-Y relative c.m. momentum ($P_Y^{c.m.}$) as a function of the incident laboratory photon energy (E_γ^{lab}) for each hyperon [$Y = \Lambda, \Sigma^0, \Lambda(1405)$]. The horizontal lines give approximate momenta where the partial waves (labeled by quantum number L) are expected to dominate the production amplitude. The points of intersection yield an approximation to the minimum photon energy necessary to excite the next higher partial wave.

fit, the K^* simulated higher-spin resonances are incapable of providing the necessary interference needed to reproduce the $\Lambda(1405)$ q^2 dependence. Assuming the effects from higher-spin resonances are being adequately simulated by these K^* graphs, it appears that the necessary interference must be due to some neglected spin-1/2 state(s). In our calculations, we have noticed significant sensitivity to u-channel interference and that an excellent fit to the $\Lambda(1405)$ data is possible by unconstraining the Born Λ and Σ graphs. However, in this case the coupling constants become unphysical, but since there are several other possible spin-1/2 u-channel resonances which have been neglected, we believe one or more of these states may be important for $\Lambda(1405)$ production.

It is interesting to note that very similar results were reported in reference [22] where an exclusively t-channel Regge pole model designed for high-energy photoproduction data, $E_\gamma = 5.0, 8.0, 11.0, 16.0$ GeV, was extrapolated to analyze much lower energy electroproduction data. They found that their model severely underpredicted the electroproduction data which motivated a subsequent analysis that considered unnatural parity exchanges to restore agreement. We believe an alternative explanation exists, related to the partial wave deficiency discussed above, involving an unphysical suppression of the lowest partial waves in their calculation. In their approach, the model amplitude is decomposed into partial waves, keeping terms with total angular momentum up to $J = 20$, which are individually multiplied by a (J dependent) suppression function (to account for final-state absorptive effects), parametrized using an energy-independent coefficient governing the magnitude of absorption (which is in general energy dependent). They achieved a good description of the high-energy data by adjusting this absorption parameter so that the lowest partial waves were "almost completely absorbed." Consequently and not surprising, their extrapolation of this same model to lower energies (where the low partial waves are important) underpredicted the data by a factor of $\sim 1/2$. Instead of introducing additional Regge trajectories to overcome the suppression, we believe an alternative approach would be to reanalyze both the high- and low-energy data using a more realistic, energy-dependent absorption parameter. Then one could assess whether additional Regge trajectories are needed. In contrast, our original model did not contain the correct high-energy physics (truncated at spin-1/2 resonances, producing only s and p waves) and so the partial wave deficiency we observe must be attributed to our neglect of higher spin resonances.

In Figs. 10, 11, and 12 the energy dependence of Λ, Σ^0, and $\Lambda(1405)$ is displayed. We find good qualitative agreement between our new model and the behavior of the data. The Σ^0 curve, although having the correct overall magnitude, has a slowly increasing W behavior whereas the data is decreasing. Also, the Λ curve shows very little W dependence while the data decreases over the same energy range. The $\Lambda(1405)$ dependence, which compares favorably with the data, is primarily due to interference from the $N(1650)$ diagram which has a large, probably unphysical effective coupling, as discussed earlier. Without this diagram, the cross section is roughly twice as large and increasing slowly whereas the data appears constant or slowly decreasing. We note that even though only semiquantitative agreement exists with the data, such results are to be expected when a truncated duality approximation is made. Including only a few t-channel diagrams, while convenient to incorporate, can only provide a gross, general description of the s-channel physics. The detailed behavior arising from many s-channel resonances can only be represented accurately by t-channel exchanges if duality is implemented exactly.

Figures 13, 14, and 15 demonstrate the t dependence for Λ , Σ^0, and $\Lambda(1405)$ production, respectively. Again, qualitative agreement has been achieved. The data marginally suggests that for $|t| > 0.15$ GeV^2 the invariant cross section declines in value for both Λ and Σ^0, which is consistent with the photoproduction angular distribu-

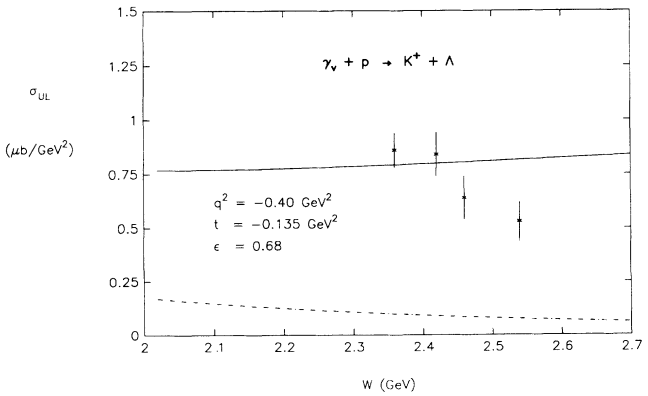

FIG. 10. σ_{UL} for Λ as a function of $W = \sqrt{s}$. Data are taken from Ref. [27].

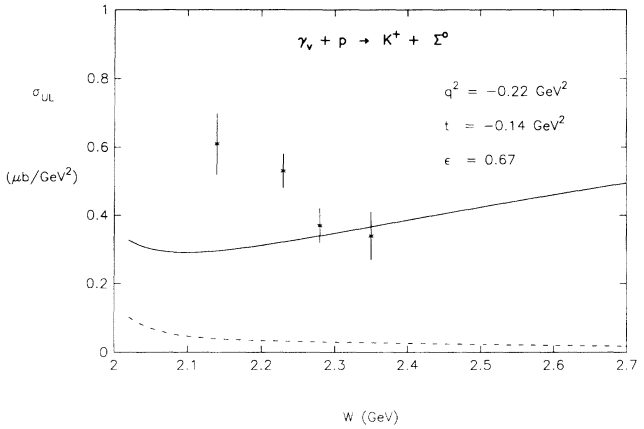

FIG. 11. σ_{UL} for Σ^0 as a function of $W = \sqrt{s}$. Data are taken from Ref. [27].

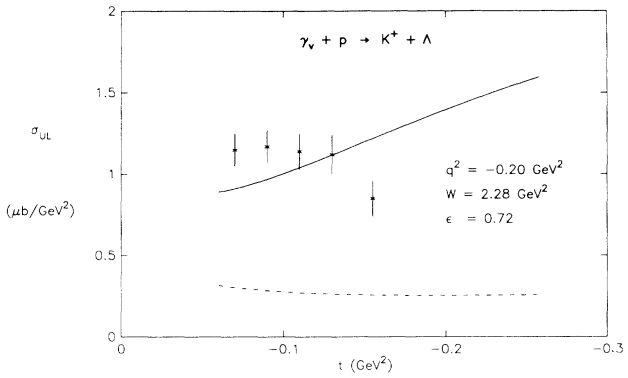

FIG. 13. σ_{UL} for Λ as a function of t. Data are taken from Ref. [27].

tions having back-angle suppression. One of the difficulties associated with including massive spin-1 mesons in a field theoretic model is that the tensor coupling of the strong interaction vertex introduces a linear t dependence in the differential cross section. At low energies, interference between the various diagrams can produce reasonable angular distributions; however, at higher energies the cancellation is incomplete and the linear t dependence dominates, producing an unphysical back angle enhancement of the cross section. This problem arises due to the pointlike effective field interactions which permit no substructure for the higher-spin hadrons in the model. Field theories are only well defined (i.e., formally renormalizable) for spin-1/2 fermions and scalar bosons (unless it is a gauge theory, in which case spin-1 bosons naturally arise and do not spoil the renormalizability). Although higher-order diagrams are not being calculated, the incorrect energy dependence associated with a nonrenormalizable field theory is present even at tree level. In principle, this problem can be circumvented by introducing a strong form factor to suppress the tensor coupling at higher energies (the energy-scale dependence of the tensor coupling is evident by its inverse mass dimension). However, based on the current quality of data and the level of agreement that we obtain, we have not pursued this approach even though at higher energies it may be unavoidable for this type of model. More fundamentally, the breakdown of this type of quantum hadrodynamic (QHD) model should not be surprising if a transition to perturbative QCD dynamics has set in. There is some experimental evidence for a transition from the s^{-2} scaling behavior consistent with hadronic model calculations to an s^{-7} behavior predicted by PQCD counting rules at about $E_\gamma \sim 2$ GeV for sufficiently large $|t|$ [23]. It is possible that the larger-$|t|$ electroproduction data is already in the transition region between QHD and PQCD, in which case the breakdown of our model is quite natural. This interesting region is very important for our understanding of nonperturbative QCD and is the focus of proposed future investigations at CEBAF [24].

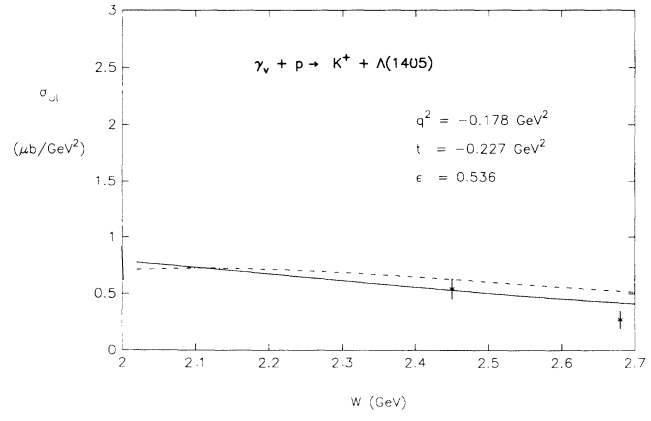

FIG. 12. σ_{UL} for $\Lambda(1405)$ as a function of $W = \sqrt{s}$. Data are taken from Ref. [27].

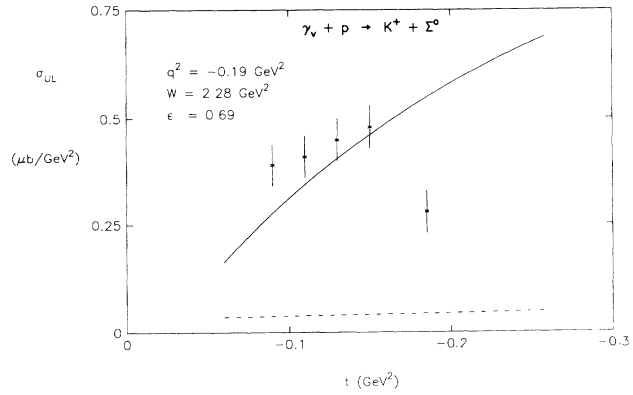

FIG. 14. σ_{UL} for Σ^0 as a function of t. Data are taken from Ref. [27].

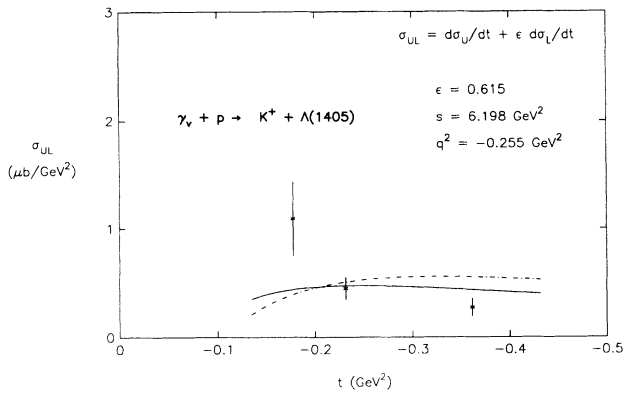

FIG. 15. σ_{UL} for $\Lambda(1405)$ as a function of t. Data are taken from Ref. [27].

V. CONCLUSIONS

In this paper we have attempted to provide a consistent and comprehensive phenomenological model for hyperon electromagnetic production processes. By simultaneously studying Λ, Σ^0, and $\Lambda(1405)$ production, we have confidence that the common hadronic and electromagnetic coupling parameters are well constrained and therefore presumably better determined. Our success in predicting the cross channel capture branching ratios using the same model strengthens our confidence that the extracted coupling constants are reliable and physical. The importance of crossing has led us to concentrate on developing covariant expressions for the spin averaged, squared amplitude, which permit a natural analytic continuation to the crossed channel. These formulas will be useful when we consider the kaon-induced pair production processes, $p(K^-, e^+e^-)Y$, in a future publication. By incorporating a duality motivated correction to a low-energy model which contains only kinematically enhanced, spin-1/2 Born and resonance graphs, we have extended the energy range where the model is applicable and ensured phenomenological efficiency by explaining an abundance of data with a minimal parameter set. The duality correction ansatz is a method for representing the collective effects of several higher-spin s- and u-channel resonances by a few t-channel exchanges. This is not only very convenient, but more importantly, it also avoids the complexity of a model having several competing resonances and the attending phenomenological uncertainties associated with a much larger parameter space. The limitation of this approach is that only gross, qualitative features of the data can be reproduced since, for a particular energy region, the detailed production mechanism is generally governed by an intricate interplay of many resonances. We anxiously await future data from CEBAF and KAON which will help clarify the details of the reaction mechanism which at the present cannot be further addressed. Furthermore, additional precision data will help provide insight concerning the speculated transition from hadronic to chromodynamic degrees of freedom at energies as low as $E_\gamma \sim 2$ GeV for sufficiently large $|t|$ [23, 24]. If the transition from hadronic, s^{-2}, to chromodynamic, s^{-7}, scaling is observed at CEBAF energies, then a PQCD analysis may be appropriate, such as the recent large scale computer calculations of Farrar *et al.* [25].

Whether or not PQCD is applicable at CEBAF is a controversial topic which should be resolved one way or the other with new precise data and additional calculations. However, everyone agrees that CEBAF will play an important role in our understanding of nonperturbative features of the strong interaction. Because QCD is (at present) unsolvable, it is important to develop phenomenological effective potential models (at both the quark and hadronic level) which avoid the complexity of the underlying QCD interactions by attempting to parametrize the nonperturbative QCD physics in a physically sensible yet tractable formalism. One obvious advantage with this type of approach is that after all parameters have been consistently determined, such a model has definite predictive power, which can then motivate and be further tested by new experiments. A novel feature of the crossing consistent model described in this paper is that in addition to being able to make definite predictions for kaon electroproduction reactions observable at CEBAF, we also have justifiable confidence in our predictions for the low energy $p(K^-, e^+e^-)Y$ reactions relevant with KAON experiments (which we detail in an upcoming work). With complimentary information coming from these reactions, we expect ongoing progress and a steady evolution in the development of a consistent and unified description of electromagnetic hyperon production.

In summary, over the last three decades of kaon electromagnetic production studies, a variety of theoretical models have been formulated. Our approach has been to represent the hyperon production amplitude in terms of a sum over tree-level Born and resonance graphs calculated from an effective field chiral Lagrangian containing phenomenological coupling constants. Hadrodynamic field theories have a long and successful history in nuclear physics, incorporate the proper symmetries, and contain the correct degrees of freedom for low-energy phenomena while providing a comprehensive, yet tractable, general framework for studying the strong interaction. One of the main advantages in this type of model is that the formalism is explicitly relativistic and covariant, naturally lending itself to a simultaneous description of crossing related reactions in several production channels. Within this general framework, we have treated Λ, Σ^0, and $\Lambda(1405)$ hyperon production in a unified and consistent way.

ACKNOWLEDGMENTS

Financial support from U.S. Department of Energy Grants Nos. DE-FG05-88ER40461 and DE-FG05-90ER40589 is gratefully acknowledged. We also thank the North Carolina Supercomputing Center for the grant of Cray Y-MP time.

APPENDIX

The different basis matrices are related by a transformation on the invariant amplitudes defined by

$$A_i \equiv R_i^j \, B_j,$$

$$B_i = (R^{-1})_i^j \, A_j,$$

hence the basis matrices transform by the inverse matrix

$$\mathcal{M}_\mu^i = (R^{-1})_j^i \, \mathcal{N}_\mu^j,$$

$$\mathcal{N}_\mu^i = R_j^i \, \mathcal{M}_\mu^j.$$

The transformation matrix and its inverse are given explicitly by

$$(R)_i^j = \begin{pmatrix} 1 & 0 & 0 & 0\,0\,0 \\ 0 & \frac{1}{2q\cdot(l-p)} & \frac{1}{2q\cdot(l-p)} & 0\,0\,0 \\ 0 & 0 & 0 & 1\,0\,0 \\ 0 & 0 & 0 & 0\,1\,0 \\ 0 & \frac{q\cdot p}{q^2 q\cdot(l-p)} & \frac{q\cdot l}{q^2 q\cdot(l-p)} & 0\,0\,0 \\ 0 & 0 & 0 & 0\,0\,1 \end{pmatrix},$$

$$(R^{-1})_i^j = \begin{pmatrix} 1 & 0 & 0\,0 & 0 & 0 \\ 0 & 2q\cdot l & 0\,0 & -q^2 & 0 \\ 0 & -2q\cdot p & 0\,0 & q^2 & 0 \\ 0 & 0 & 1\,0 & 0 & 0 \\ 0 & 0 & 0\,1 & 0 & 0 \\ 0 & 0 & 0\,0 & 0 & 1 \end{pmatrix}.$$

Furthermore, this transformation can be used to relate the traces obtained using the different bases:

$$< |t_{fi}|^2 > \propto \sum_{i,j=1}^{6} A_i \, A_j^* \, [\, T_1^{ij} + T_2^{ij}] = \sum_{i,j=1}^{6} B_i \, B_j^* \, [\, \bar{T}_1^{ij} + \bar{T}_2^{ij}]$$

where

$$T_1^{ij} \equiv \mathbf{Tr}\, [(\not{l} + M_Y)\mathcal{M}_\mu^i(\not{p} + M_p)\mathcal{M}_\nu^{j^\dagger} \, g^{\mu\nu}\,],$$

$$T_2^{ij} \equiv (\frac{4}{q^2})\, \mathbf{Tr}\, [(\not{l} + M_Y)(\mathcal{M}^i \cdot e_1)(\not{p} + M_p)(\mathcal{M}^{j^\dagger} \cdot e_1)],$$

$$\bar{T}_1^{ij} \equiv \mathbf{Tr}\, [(\not{l} + M_Y)\mathcal{N}_\mu^i(\not{p} + M_p)\mathcal{N}_\nu^{j^\dagger} \, g^{\mu\nu}\,],$$

$$\bar{T}_2^{ij} \equiv (\frac{4}{q^2})\, \mathbf{Tr}\, [(\not{l} + M_Y)(\mathcal{N}^i \cdot e_1)(\not{p} + M_p)(\mathcal{N}^{j^\dagger} \cdot e_1)],$$

hence,

$$\bar{T}_q^{kl} = \sum_{i,j=1}^{6} R_i^k \, R_j^l \, T_q^{ij},$$

$(\, i,j,k,l = 1,2,...,6;\; q = 1,2\,)$.

The traces have been performed using REDUCE and found to be consistent with our hand calculations. Explicitly, we find for the Hermitian $T_1^{ij}(\pm)$ and $T_2^{ij}(\pm)$ matrix elements (where the $\pm$ labels the produced hyperon parity):

$$T_1^{1,1}(\pm) = 16 l\cdot q p\cdot q + 4q^2(\pm 3 M_Y M_p - p\cdot l),$$

$$T_1^{1,2}(\pm) = -8[M_Y^2 (p\cdot q)^2 + M_p^2 (l\cdot q)^2 - 2p\cdot l\, l\cdot q p\cdot q],$$

$$T_1^{1,3}(\pm) = -4M_p q^2 (p\cdot l \pm M_Y M_p) - 8 p\cdot q (M_p l\cdot q \pm M_Y p\cdot q),$$

$$T_1^{1,4}(\pm) = -(\pm) 4 M_Y q^2 (p\cdot l \pm M_Y M_p) - 8 l\cdot q (M_p l\cdot q \pm M_Y p\cdot q),$$

$$T_1^{1,5}(\pm) = -4q^2[l\cdot q(p\cdot l - M_p^2) + p\cdot q(p\cdot l - M_Y^2)],$$

$$T_1^{1,6}(\pm) = 12 q^2 (M_p l\cdot q \pm M_Y p\cdot q),$$

$$T_1^{2,2}(\pm) = -16(p\cdot l \pm M_Y M_p)[M_Y^2(p\cdot q)^2 + M_p^2(l\cdot q)^2 - 2p\cdot ql\cdot qp\cdot l],$$
$$T_1^{2,3}(\pm) = -8M_p[2p\cdot ql\cdot qp\cdot l - M_Y^2(p\cdot q)^2 - M_p^2(l\cdot q)^2],$$
$$T_1^{2,4}(\pm) = -(\pm)8M_Y[2p\cdot ql\cdot qp\cdot l - M_Y^2(p\cdot q)^2 - M_p^2(l\cdot q)^2],$$
$$T_1^{2,5}(\pm) = 8q^2(p\cdot l - (\pm)M_Y M_p)[M_Y^2 p\cdot q + M_p^2 l\cdot q - p\cdot l(p\cdot q + l\cdot q)],$$
$$T_1^{2,6}(\pm) = 8q^2(p\cdot l - (\pm)M_Y M_p)[M_p l\cdot q \pm M_Y p\cdot q],$$
$$T_1^{3,3}(\pm) = 4(p\cdot l \pm M_Y M_p)[2(p\cdot q)^2 + q^2 M_p^2],$$
$$T_1^{3,4}(\pm) = 4(M_p l\cdot q \pm M_Y p\cdot q)^2 + 4p\cdot l(p\cdot l \pm M_Y M_p),$$
$$T_1^{3,5}(\pm) = -4M_p q^2[l\cdot q(M_p^2 - p\cdot l) + p\cdot q(M_Y^2 - p\cdot l)],$$
$$T_1^{3,6}(\pm) = -4q^2[p\cdot q(\pm 3M_Y M_p + 2p\cdot l) + M_p^2 l\cdot q],$$
$$T_1^{4,4}(\pm) = 4(p\cdot l \pm M_Y M_p)[2(l\cdot q)^2 + q^2 M_Y^2],$$
$$T_1^{4,5}(\pm) = \pm 4M_Y q^2[l\cdot q(p\cdot l - M_p^2) + p\cdot q(p\cdot l - M_Y^2)],$$
$$T_1^{4,6}(\pm) = -4q^2[l\cdot q(\pm 3M_Y M_p + 2p\cdot l) + M_Y^2 p\cdot q],$$
$$T_1^{5,5}(\pm) = -4q^2(p\cdot l - (\pm)M_Y M_p)[q^2(M_p^2 + M_Y^2 - 2p\cdot l) + 2p\cdot ql\cdot q - (p\cdot q)^2 - (l\cdot q)^2],$$
$$T_1^{5,6}(\pm) = -4q^2[q^2(M_p \pm M_Y)(p\cdot l - (\pm)M_Y M_p) - q\cdot(p-l)(M_p l\cdot q - (\pm)M_Y p\cdot q)],$$
$$T_1^{6,6}(\pm) = 4q^2[2p\cdot ql\cdot q + q^2(\pm 3M_Y M_p + p\cdot l)],$$

$$T_2^{1,1}(\pm) = -(\frac{16}{q^2})(\pm M_Y M_p - l\cdot p)[(q\cdot e_1)^2 - q^2 M_e^2]$$
$$-32(\frac{l\cdot q}{q^2})(p\cdot e_1 q\cdot e_1 - M_e^2 p\cdot q) - 32(\frac{l\cdot e_1}{q^2})(p\cdot qq\cdot e_1 - q^2 p\cdot e_1),$$
$$T_2^{1,2}(\pm) = -(\frac{32}{q^2})(l\cdot e_1 p\cdot q - l\cdot qp\cdot e_1)^2,$$

$$T_2^{1,3}(\pm) = -(\frac{16}{q^2})[(p\cdot e_1 q^2 - p\cdot qq\cdot e_1)(\pm M_Y p\cdot e_1 + M_p l\cdot e_1)$$
$$+(M_e^2 p\cdot q - p\cdot e_1 q\cdot e_1)(\pm M_Y p\cdot q + M_p l\cdot q)],$$

$$T_2^{1,4}(\pm) = -(\frac{16}{q^2})[(l\cdot e_1 q^2 - l\cdot qq\cdot e_1)(M_p l\cdot e_1 \pm M_Y p\cdot e_1)$$
$$+(M_e^2 l\cdot q - l\cdot e_1 q\cdot e_1)(M_p l\cdot q \pm M_Y p\cdot q)],$$
$$T_2^{1,5}(\pm) = -(\frac{16}{q^2})(l\cdot e_1 p\cdot q - l\cdot qp\cdot e_1)[q^2 e_1\cdot(p-l) - q\cdot e_1 q\cdot(p-l)],$$
$$T_2^{1,6}(\pm) = -(\frac{16}{q^2})(M_p l\cdot q \pm M_Y p\cdot q)[(q\cdot e_1)^2 - q^2 M_e^2],$$
$$T_2^{2,2}(\pm) = -(\frac{64}{q^2})(p\cdot l - \pm M_Y M_p)(p\cdot ql\cdot e_1 - l\cdot qp\cdot e_1)^2,$$
$$T_2^{2,3}(\pm) = (\frac{32M_p}{q^2})(l\cdot qp\cdot e_1 - p\cdot ql\cdot e_1)^2,$$
$$T_2^{2,4}(\pm) = (\frac{\pm 32M_Y}{q^2})(l\cdot qp\cdot e_1 - p\cdot ql\cdot e_1)^2,$$
$$T_2^{2,5}(\pm) = -(\frac{32}{q^2})(p\cdot l - (\pm)M_Y M_p)[(p\cdot ql\cdot e_1 - l\cdot qp\cdot e_1)(q\cdot e_1 q\cdot(p-l) - q^2 e_1\cdot(p-l))],$$
$$T_2^{2,6}(\pm) = -(\frac{32}{q^2})(l\cdot qp\cdot e_1 - p\cdot ql\cdot e_1)[\pm M_Y(q^2 p\cdot e_1 - p\cdot qq\cdot e_1) - M_p(q^2 l\cdot e_1 - l\cdot qq\cdot e_1)],$$
$$T_2^{3,3}(\pm) = -(\frac{16}{q^2})(p\cdot l \pm M_Y M_p)[p\cdot q(p\cdot e_1 q\cdot e_1 - M_e^2 p\cdot q) + p\cdot e_1(p\cdot qq\cdot e_1 - q^2 p\cdot e_1)],$$
$$T_2^{3,4}(\pm) = (\frac{16}{q^2})(l\cdot qp\cdot e_1 - p\cdot ql\cdot e_1)^2$$
$$-(\frac{16}{q^2})(p\cdot l \pm M_Y M_p)[p\cdot q(l\cdot e_1 q\cdot e_1 - M_e^2 l\cdot q) + p\cdot e_1(l\cdot qq\cdot e_1 - l\cdot e_1 q^2)],$$

$$T_2^{3,5}(\pm) = -(\frac{16M_p}{q^2})(l\cdot qp\cdot e_1 - p\cdot ql\cdot e_1)[q^2 e_1\cdot(p-l) - q\cdot e_1 q\cdot(p-l)],$$

$$T_2^{3,6}(\pm) = 16(\frac{p\cdot q}{q^2})(p\cdot l \pm M_Y M_p)[(q\cdot e_1)^2 - q^2 M_e^2] - (\frac{16}{q^2})(p\cdot qq\cdot e_1 - q^2 p\cdot e_1)(p\cdot ql\cdot e_1 - l\cdot qp\cdot e_1),$$

$$T_2^{4,4}(\pm) = -(\frac{16}{q^2})(p\cdot l \pm M_Y M_p)[l\cdot q(l\cdot e_1 q\cdot e_1 - M_e^2 l\cdot q) + l\cdot e_1(l\cdot qq\cdot e_1 - q^2 l\cdot e_1)],$$

$$T_2^{4,5}(\pm) = -(\frac{\pm 16M_Y}{q^2})(l\cdot qp\cdot e_1 - p\cdot ql\cdot e_1)[q^2 e_1\cdot(p-l) - q\cdot e_1 q\cdot(p-l))],$$

$$T_2^{4,6}(\pm) = 16(\frac{l\cdot q}{q^2})(p\cdot l \pm M_Y M_p)[(q\cdot e_1)^2 - q^2 M_e^2] - (\frac{16}{q^2})(l\cdot qq\cdot e_1 - q^2 l\cdot e_1)(l\cdot qp\cdot e_1 - p\cdot ql\cdot e_1),$$

$$T_2^{5,5}(\pm) = -(\frac{16}{q^2})(p\cdot l - (\pm)M_Y M_p)[q\cdot(p-l)q\cdot e_1 - q^2 e_1\cdot(p-l)]^2,$$

$$T_2^{5,6}(\pm) = -(\frac{16}{q^2})[q\cdot e_1 q\cdot(p-l) - q^2 e_1\cdot(p-l)][q\cdot e_1(M_p l\cdot q - (\pm)M_Y p\cdot q) - q^2(M_p l\cdot e_1 - (\pm)M_Y p\cdot e_1)],$$

$$T_2^{6,6}(\pm) = -16(p\cdot l \pm M_Y M_p)[(q\cdot e_1)^2 - q^2 M_e^2] - (\frac{32}{q^2})(p\cdot qq\cdot e_1 - q^2 p\cdot e_1)(l\cdot qq\cdot e_1 - q^2 l\cdot e_1).$$

These matrix elements are functions of the kinematic invariants formed by products of the available 4-momenta. For completeness, we list expressions for the 4-vector components in both the laboratory and c.m. systems. The laboratory system ($\mathbf{p} = 0$):

$$q_{\rm lab} = (q_0', 0, 0, |\mathbf{q}'|),$$
$$p_{\rm lab} = (M_p, 0, 0, 0),$$
$$k_{\rm lab} = (k_0', 0, |\mathbf{k}'|\sin\theta', |\mathbf{k}'|\cos\theta')$$
$$l_{\rm lab} = (l_0', 0, -|\mathbf{k}'|\sin\theta', \mathbf{q}' - |\mathbf{k}'|\cos\theta').$$

The (γp) c.m. system ($\mathbf{q} + \mathbf{p} = \mathbf{k} + \mathbf{l} = 0$):

$$q_{\rm c.m.} = (q_0, 0, 0, |\mathbf{q}|),$$
$$p_{\rm c.m.} = (p_0, 0, 0, -|\mathbf{q}|),$$
$$k_{\rm c.m.} = (k_0, 0, |\mathbf{k}|\sin\theta, |\mathbf{k}|\cos\theta),$$
$$l_{\rm c.m.} = (l_0, 0, -|\mathbf{k}|\sin\theta, -|\mathbf{k}|\cos\theta).$$

The leptonic 4-vectors are determined from the photon's 4-momentum and the scattering angles Ψ and α defined in Fig. 2. The following expressions are valid in either system:

$$e_1 \equiv (e_0, e_x, e_y, e_z),$$
$$e_2 \equiv (e_0', e_x', e_y', e_z'),$$

where

$$e_0 = \frac{q_0}{2}[\,1 + (1 - \frac{q^2}{q_0^2\sin^2\frac{\Psi}{2}})^{1/2}\,]$$
$$= \frac{1}{2}[\,q_0 + |\mathbf{q}|(\frac{1+\epsilon}{1-\epsilon})^{1/2}\,],$$
$$e_0' = e_0 - q_0$$
$$= \frac{1}{2}[\,-q_0 + |\mathbf{q}|(\frac{1+\epsilon}{1-\epsilon})^{1/2}\,],$$

$$e_z = |\mathbf{e}|\cos\alpha, \qquad e_z' = e_z - |\mathbf{q}|,$$
$$e_y \Rightarrow 0, \qquad e_y' = e_y,$$
$$e_x = |\mathbf{e}|\sin\alpha, \qquad e_x' = e_x,$$

and neglecting the electron mass

$$|\mathbf{e}| \overset{M_e^2\to 0}{\Longrightarrow} e_0,$$

$$\cos\alpha \equiv \frac{e_z}{(e_x^2 + e_z^2)^{1/2}}$$
$$= \frac{q_0}{|\mathbf{q}|}(1 - \frac{q^2}{2e_0 q_0}),$$
$$\sin\alpha \equiv \frac{e_x}{(e_x^2 + e_z^2)^{1/2}}$$
$$= [\,1 - \frac{q_0^2}{|\mathbf{q}|^2}(1 - \frac{q^2}{2e_0 q_0})^2]^{1/2}.$$

The 4-momentum components are functions of the Mandelstam variables:

$$s \equiv (q+p)^2 \equiv (k+l)^2,$$
$$t \equiv (p-l)^2 \equiv (k-q)^2,$$
$$u \equiv (q-l)^2 \equiv (k-p)^2,$$

and are given by

$$q_0 = \frac{s + q^2 - M_p^2}{2\sqrt{s}}, \quad q_0' = \frac{(s - M_p^2 - q^2)}{2M_p},$$
$$p_0 = \frac{s - q^2 + M_p^2}{2\sqrt{s}}, \quad p_0' = M_p,$$
$$k_0 = \frac{s - M_Y^2 + M_K^2}{2\sqrt{s}}, \quad k_0' = \frac{(M_p^2 + M_K^2 - u)}{2M_p},$$
$$l_0 = \frac{s + M_Y^2 - M_K^2}{2\sqrt{s}}, \quad l_0' = \frac{(M_p^2 + M_Y^2 - t)}{2M_p},$$

with

$$|\mathbf{q}| = (q_0^2 - q^2)^{1/2}, \quad |\mathbf{q}'| = (q_0'^2 - q^2)^{1/2},$$
$$|\mathbf{k}| = (k_0^2 - M_K^2)^{1/2}, \quad |\mathbf{k}'| = (k_0'^2 - M_K^2)^{1/2},$$

and the transformation between the lab and c.m. kaon angle given by

$$\cos\theta' = \cos\theta\,[\frac{|\mathbf{q}|\,|\mathbf{k}|\,(q_0'k_0' - q\cdot k)}{|\mathbf{q}'|\,|\mathbf{k}'|\,(q_0k_0 - q\cdot k)}]$$

Expressions for the invariant products appearing in the T^{ij} elements are

$$q\cdot p = \frac{1}{2}(s - M_p^2 - q^2),$$
$$q\cdot k = \frac{1}{2}(q^2 + M_K^2 - t),$$
$$q\cdot l = \frac{1}{2}(q^2 + M_Y^2 - u),$$
$$p\cdot l = \frac{1}{2}(M_p^2 + M_Y^2 - t),$$
$$p\cdot k = \frac{1}{2}(M_p^2 + M_K^2 - u),$$
$$k\cdot l = \frac{1}{2}(s - M_K^2 - M_Y^2).$$

and the leptonic invariants (evaluated in the laboratory system):

$$q\cdot e_1 = e_0(q_0' - |\mathbf{q}'|\cos\alpha),$$
$$p\cdot e_1 = e_0 M_p,$$
$$l\cdot e_1 = e_0[\,l_0' + |\mathbf{k}'|\sin\theta'\cos\phi\sin\alpha - (|\mathbf{q}'| - |\mathbf{k}'|\cos\theta')\cos\alpha\,],$$
$$k\cdot e_1 = e_0[\,k_0' - |\mathbf{k}'|\sin\theta'\mathbf{q}'\cos\phi\sin\alpha - |\mathbf{k}'|\cos\theta'\cos\alpha\,].$$

The invariant amplitudes (B_j) defined in the text are obtained by applying the Feynman rules to the graphs displayed in Fig. 1. The result of this calculation gives for the production of an even parity hyperon (i.e., $Y = \Lambda, \Sigma^0$) for Born graphs ($p, K^+, \Lambda, \Sigma^0$):

$$B_1^{\text{Born}} = \frac{g_{KNY}(e + 2M_p\mu_p)}{s - M_p^2} + \frac{\mu_{Y\Lambda\gamma}g_{KN\Lambda}(M_\Lambda \pm M_Y)}{u - M_\Lambda^2} + \frac{\mu_{Y\Sigma\gamma}g_{KN\Sigma}(M_\Sigma \pm M_Y)}{u - M_\Sigma^2},$$
$$B_2^{\text{Born}} = \frac{2eg_{KNY}(q^2 + M_Y^2 - u)}{(s - M_p^2)(t - M_K^2)},$$
$$B_3^{\text{Born}} = \frac{-2eg_{KNY}}{t - M_K^2},$$
$$B_4^{\text{Born}} = \frac{2\mu_p g_{KNY}}{s - M_p^2},$$
$$B_5^{\text{Born}} = \frac{2\mu_{Y\Lambda\gamma}g_{KN\Lambda}}{u - M_\Lambda^2} + \frac{2\mu_{Y\Sigma\gamma}g_{KN\Sigma}}{u - M_\Sigma^2},$$
$$B_6^{\text{Born}} = \frac{-\mu_p g_{KNY}}{s - M_p^2} + \frac{\mu_{Y\Lambda\gamma}g_{KN\Lambda}}{u - M_\Lambda^2} + \frac{\mu_{Y\Sigma\gamma}g_{KN\Sigma}}{u - M_\Sigma^2};$$

for s-channel graphs (N^*):

$$B_1^{N^*(\frac{1}{2}\pm)} = \frac{\mu_{N^*p\gamma}g_{KN^*Y}(M_{N^*} \pm M_p - i\frac{\Gamma_{N^*}}{2})}{s - M_{N^*}^2 + iM_{N^*}\Gamma_{N^*}},$$
$$B_2^{N^*(\frac{1}{2}\pm)} = 0,$$
$$B_3^{N^*(\frac{1}{2}\pm)} = 0,$$
$$B_4^{N^*(\frac{1}{2}\pm)} = \frac{\pm 2\mu_{N^*p\gamma}g_{KN^*Y}}{s - M_{N^*}^2 + iM_{N^*}\Gamma_{N^*}},$$
$$B_5^{N^*(\frac{1}{2}\pm)} = 0,$$
$$B_6^{N^*(\frac{1}{2}\pm)} = \frac{-(\pm)\,\mu_{N^*p\gamma}g_{KN^*Y}}{s - M_{N^*}^2 + iM_{N^*}\Gamma_{N^*}}.$$

The s-channel $\Delta^*(\frac{1}{2}\pm)$ invariant amplitude formulae associated with Σ^0 production have the same form as the $N^*(\frac{1}{2}\pm)$, hence they are trivially generated by mass, width, and coupling constant substitutions into the above expressions.

for t-channel graphs (K^*):

$$B_1^{K^*(1\pm)} = \frac{[1 \pm (-1)]\,g_{K^*K\gamma}}{2M(t - M_{K^*}^2 + iM_{K^*}\Gamma_{K^*})}[g_{K^*NY}^V(M_Y + M_p) + \frac{g_{K^*NY}^T}{2M_p}t\,],$$

$$B_2^{K^*(1\pm)} = \frac{-(\pm)g_{K^*K\gamma}g^T_{K^*NY}}{2MM_p(t-M^2_{K^*}+iM_{K^*}\Gamma_{K^*})}(q^2+M_Y^2-u)\,,$$

$$B_3^{K^*(1\pm)} = \frac{\pm g_{K^*K\gamma}g^T_{K^*NY}}{2MM_p(t-M^2_{K^*}+iM_{K^*}\Gamma_{K^*})}(s-q^2-M_p^2)\,,$$

$$B_4^{K^*(1\pm)} = \frac{g_{K^*K\gamma}}{M(t-M^2_{K^*}+iM_{K^*}\Gamma_{K^*})}[g^V_{K^*NY}\pm(\frac{M_Y-M_p}{2M_p})g^T_{K^*NY}]\,,$$

$$B_5^{K^*(1\pm)} = \frac{-(\pm)g_{K^*K\gamma}}{M(t-M^2_{K^*}+iM_{K^*}\Gamma_{K^*})}[g^V_{K^*NY}+(\frac{M_Y-M_p}{2M_p})g^T_{K^*NY}]\,,$$

$$B_6^{K^*(1\pm)} = 0;$$

for u-channel graphs (Y^*):

$$B_1^{Y^*(\frac{1}{2}\pm)} = \frac{\mu_{Y^*Y\gamma}g_{KNY^*}(M_{Y^*}\pm M_Y - i\frac{\Gamma_{Y^*}}{2})}{u-M^2_{Y^*}+iM_{Y^*}\Gamma_{Y^*}}\,,$$

$$B_2^{Y^*(\frac{1}{2}\pm)} = 0\,,$$

$$B_3^{Y^*(\frac{1}{2}\pm)} = 0\,,$$

$$B_4^{Y^*(\frac{1}{2}\pm)} = 0\,,$$

$$B_5^{Y^*(\frac{1}{2}\pm)} = \frac{\pm 2\mu_{Y^*Y\gamma}g_{KNY^*}}{u-M^2_{Y^*}+iM_{Y^*}\Gamma_{Y^*}}\,,$$

$$B_6^{Y^*(\frac{1}{2}\pm)} = \frac{\pm\mu_{Y^*Y\gamma}g_{KNY^*}}{u-M^2_{Y^*}+iM_{Y^*}\Gamma_{Y^*}}\,.$$

To obtain the invariant amplitudes for the production of an odd parity hyperon, such as $Y=\Lambda(1405)$, simply make the following replacement everywhere:

$$B_j(M_Y)\rightarrow B_j(-M_Y).$$

The total amplitude is a sum of contributions from each diagram:

$$B_j(q^2,s,t,u) = B_j^{\rm Born}(q^2,s,t,u)+\sum_{N^*}B_j^{N^*}(q^2,s,t,u)+\sum_{Y^*}B_j^{Y^*}(q^2,s,t,u)+\{\sum_{K^*}B_j^{K^*}(q^2,s,t,u)\}_{\substack{\rm Duality\\ \rm correction}}$$

where the low-lying t-channel K^* resonances have been included to give a duality motivated correction to the truncated amplitude (spin-1/2 limited s- and u-channel graphs).

[1] Robert A. Williams, Chueng-Ryong Ji, and Stephen R. Cotanch, Phys. Rev. C **43**, 452 (1991).

[2] Robert A. Williams, Chueng-Ryong Ji, and Stephen R. Cotanch, Phys. Rev. D **41**, 1449 (1990).

[3] R. Dolen, D. Horn, and C. Schmid, Phys. Rev. Lett. **19**, 402 (1967); Phys. Rev. **166**, 1768 (1968).

[4] G. Veneziano, Nuovo Cimento A **57**, 190 (1968).

[5] M. Fukugita and K. Igi, Phys. Lett. **31C**, 237 (1977).

[6] V. De Alfaro, S. Fubini, G. Furlan, and C. Rossetti, *Currents in Hadron Physics* (North-Holland, Amsterdam, 1972), pp. 571–662.

[7] F. M. Renard and Y. Renard, Nucl. Phys. **B25**, 490 (1971); Y. Renard, *ibid.* **B40**, 499 (1972).

[8] W. Schorsch, J. Tietge, and W. Weilnbock, Nucl. Phys. **B25** 179 (1970).

[9] R. A. Adelseck and B. Saghai, Phys. Rev. C **42**, 108 (1990); R. A. Adelseck and L. E. Wright, *ibid.* **38**, 1965 (1989).

[10] C.-R. Ji and S. R. Cotanch, Phys. Rev. C **38**, 2691 (1988).

[11] D. A. Whitehouse *et al.*, Phys. Rev. Lett. **63**, 1352 (1989).

[12] G. Y. Korenman and V. P. Popov, Phys. Lett. **40B**, 628 (1972); J. O. Eeg and H. Pilkuhn, Nuovo Cimento A **32**, 44 (1976); H. Burkhardt *et al.*, Nucl. Phys. **A440**, 653 (1985); J. W. Darewych *et al.*, Phys. Rev. D **32**, 1765 (1986); K. Maltman and N. Isgur, *ibid.* **34**, 1372 (1986); R. L. Workman and H. W. Fearing, *ibid.* **37**, 3117 (1988); Y. S. Zhong *et al.*, *ibid.* **38**, 837 (1988); H. Burkhardt and J. Lowe, Phys. Rev. C **44**, 607 (1991).

[13] J. S. Ball, Phys. Rev. **124**, 2014 (1961); P. Dennery, *ibid.* **124**, 2000 (1961); M. Gourdin, Nuovo Cimento **21**, 1094 (1961); F. A. Berends *et al.*, Nucl. Phys. **B4**, 1 (1967).

[14] Shian-Shyong Hsiao, Ph.D. thesis, North Carolina State University, 1986; Nucl. Phys. **A450**, 419c (1986).

[15] M. F. Gari and W. Krumpelmann, Z. Phys. A **322**, 689 (1985); Phys. Lett. B **173**, 10 (1986); Phys. Rev. D **45**, 1817 (1992).

[16] M. Gourdin, Phys. Lett. **11C**, 29 (1974).

[17] F. Felicetti and Y. Srivastava, Phys. Lett. **107B**, 227 (1981).

[18] C. L. Hammer, T. A. Weber, and V. S. Zidell, Phys. Rev. D **9**, 158 (1974).

[19] J. J. Sakurai, Ann. Phys. (N.Y.) **11**, 1 (1960).
[20] B. Holzenkamp, K. Holinde, and J. Speth, Nucl. Phys. **A500**, 485 (1989).
[21] J. M. Lagett, Phys. Lett. B **259**, 24 (1991).
[22] N. Levy, W. Majerotto, and B. J. Read, Nucl. Phys. **B55**, 493 (1973); N. Levy *et al.*, *ibid.* **B55**, 513 (1973); A. Bartl and W. Majerotto, *ibid.* **B90**, 285 (1975).
[23] R. L. Anderson *et al.*, Phys. Rev. D **14**, 679 (1976); A. M. Boyarski *et al.*, Phys. Rev. Lett. **22**, 1131 (1969).
[24] J. Napolitano *et al.*, CEBAF proposal to PAC5, 1991, private communication.
[25] Glennys R. Farrar *et al.*, Nucl. Phys. **B349**, 655 (1991).
[26] P. Feller *et al.*, Nucl. Phys. **B39**, 413 (1972).
[27] T. Azemoon *et al.*, Nucl. Phys. **B95**, 77 (1975).

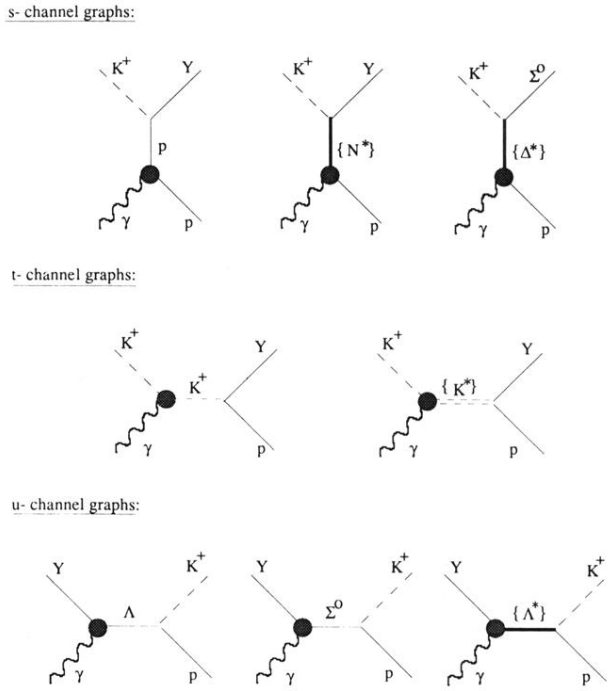

FIG. 1. Diagrams used in our model for (γ, K^+) and (K^-, γ). $\{N^*\} \equiv \{N(1650),\ N(1710)\}$, $\{\Lambda^*\} \equiv \{\Lambda(1405)\}$, $\{\Delta^*\} \equiv \{\Delta(1620),\ \Delta(1900),\ \Delta(1910)\}$, $\{K^*\} \equiv \{K^*(892),\ K_1(1270)\}$.

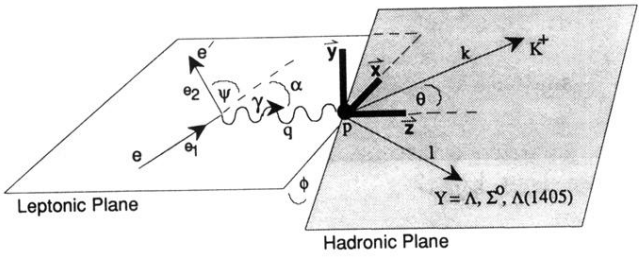

FIG. 2. Laboratory frame kinematics for electroproduction.

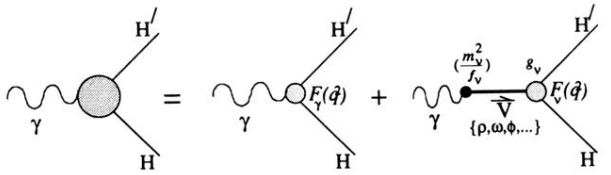

FIG. 3. Extended vector meson dominance (EVMD) picture of a physical photon coupling to a hadron.